NASA TECHNICAL NOTE

NASA TN D-3419

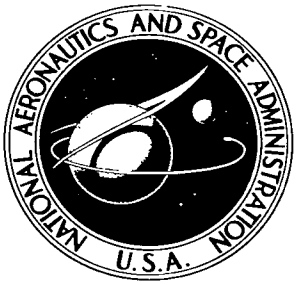

NASA TN D-3419

AN INVESTIGATION AT MACH NUMBERS FROM 0.40 TO 1.00 OF A MODEL WITH A WING HAVING INBOARD SECTIONS CAMBERED FOR MACH 1.2

by Richard J. Re and Gunars Stumbris

Langley Research Center
Langley Station, Hampton, Va.

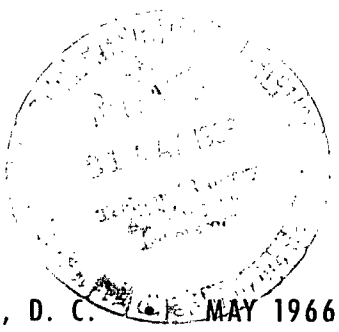

NATIONAL AERONAUTICS AND SPACE ADMINISTRATION • WASHINGTON, D. C. • MAY 1966

NASA TN D-3419

AN INVESTIGATION AT MACH NUMBERS FROM 0.40 TO 1.00 OF A MODEL WITH A WING HAVING INBOARD SECTIONS CAMBERED FOR MACH 1.2

By Richard J. Re and Gunars Stumbris

Langley Research Center
Langley Station, Hampton, Va.

NATIONAL AERONAUTICS AND SPACE ADMINISTRATION

For sale by the Clearinghouse for Federal Scientific and Technical Information
Springfield, Virginia 22151 – Price $2.00

AN INVESTIGATION AT MACH NUMBERS FROM 0.40 TO 1.00 OF A MODEL WITH A WING HAVING INBOARD SECTIONS CAMBERED FOR MACH 1.2

By Richard J. Re and Gunars Stumbris
Langley Research Center

SUMMARY

The longitudinal aerodynamic characteristics of a wing-body-tail combination with a wing designed for high efficiency at high subsonic speeds have been determined. The wing had a leading-edge sweep discontinuity at the midsemispan and was cambered for a lift coefficient of 0.4. The camber lines were calculated by using linearized theory and assuming a Mach number of 1.2 for the inboard section and a Mach number of 1.0 for the outboard section. Other model components were a cylindrical body with an ellipsoidal nose, horizontal and vertical tails, and wing fences.

Model forces and moments were determined for Mach numbers from 0.40 to 1.00 at angles of attack in the range -5° to 15°. The Reynolds number of the tests based on wing reference chord varied from 1.9×10^6 to 3.1×10^6. Boundary-layer transition was fixed for all model configurations. When compared with a similar wing-body combination, the wing-body combination of the present investigation showed an improvement in drag due to lift at Mach numbers from about 0.80 to 0.90. Streamwise fences at the wing leading-edge sweep discontinuity reduced the nonlinearity of the pitching-moment curves of the wing-body-tail combination at high lift coefficients.

INTRODUCTION

Previous investigations at high subsonic speeds of transport airplane wings with relatively high aspect ratios and sweepback angles have shown that some delay in model drag rise could be obtained by the addition of wing inboard leading-edge extensions. On the wing of reference 1, inboard leading-edge extensions which had straight camber-line segments tangent to the original camber lines at the point of maximum section thickness were added from the wing root to the midsemispan. This modification delayed the drag rise and improved the lift-drag characteristics of the model above a Mach number of about 0.85. Attempts to further improve the lift-drag characteristics of the model through the use of a wing trailing-edge modification were unsuccessful. (See ref. 2.) Pressure measurements made at the wing-body juncture during the tests of reference 1

indicated the presence of a supersonic flow field in the vicinity of the root airfoil sections at Mach numbers of 0.90 and above. It was felt, therefore, that a wing having inboard sections cambered for supersonic flow would have better lift-drag characteristics.

The wing of the present investigation was designed for a lift coefficient of 0.4 with supersonic camber lines for the inboard portion of the wing, and sonic camber lines in the vicinity of the midsemispan and for the outboard portion of the wing. The camber lines were calculated for trapezoidal chordwise loadings on the inboard portion of the wing changing gradually to rectangular loadings at the wing midsemispan and remaining rectangular to the wing tip. Spanwise and chordwise fairings of the camber lines were required, especially in the vicinity of the midsemispan, to form a smooth camber surface. Since the calculated camber lines indicated some irregularities in the vicinity of the wing midsemispan, a simple full-chord wing fence was located there to determine its effect on the wing characteristics.

The investigation was conducted at Mach numbers from 0.40 to 1.00 and at angles of attack in the range -5° to 15°. The Reynolds number of the tests, based on the wing reference chord, varied from 1.9×10^6 to 3.1×10^6.

SYMBOLS

A	aspect ratio of basic wing without inboard leading-edge chord extension, $\frac{b^2}{S} = 8.0$
A_m	model cross-sectional area
b	wing span
C_D	drag coefficient, $\frac{\text{Drag}}{qS}$
$C_{D,M}$	minimum drag coefficient
C_L	lift coefficient, $\frac{\text{Lift}}{qS}$
$C_{L,M}$	lift coefficient at $C_{D,M}$
C_{L_α}	lift-curve slope, per deg
C_m	pitching-moment coefficient about quarter-chord point of $\bar{c}$, $\frac{\text{Pitching moment}}{qS\bar{c}}$

$C_{m_{C_L}}$ static-longitudinal-stability parameter

$C_{m,o}$ pitching-moment coefficient at zero lift

C_p pressure coefficient

$C_{p,b}$ base pressure coefficient, $\frac{p_b - p_\infty}{q}$

c local wing chord, streamwise

$\bar{c}$ mean aerodynamic chord of basic wing without inboard leading-edge chord extension (reference chord), 21.85 cm (8.60 in.)

c_l section lift coefficient

i_t angle of incidence of horizontal tail, deg

k_M drag-due-to-lift factor, $\frac{\partial C_D}{\partial C_L{}^2}$

L/D lift-drag ratio

$(L/D)_{max}$ untrimmed maximum lift-drag ratio

l body length (normalizing length), 163.42 cm (64.34 in.)

M free-stream Mach number

p_b pressure at model base

p_∞ free-stream static pressure

q free-stream dynamic pressure

R straight cylindrical body radius (normalizing radius), 7.70 cm (3.03 in.)

r local radius

S area of basic wing without inboard leading-edge chord extension (reference area), 0.3173m^2 (3.415 ft^2)

x	streamwise coordinate from leading edge of local chord, positive in rearward direction
x'	coordinate measured along body center line (positive in rearward direction with tip of nose as origin)
y	spanwise coordinate measured from vertical plane through body center line
z	vertical coordinate measured with respect to horizontal line through leading edge of local chord, positive in upward direction
α	angle of attack of body center line, deg

MODEL AND APPARATUS

Model

A photograph showing the model mounted in the test section of the Langley 16-foot tunnel is presented in figure 1. Model geometry is shown in figures 2 and 3 and the model cross-sectional-area distribution is shown in figure 4.

Wing.- The wing which had a planform aspect ratio of 6.83 had leading-edge sweep of 51.34° out to the midsemispan, 42.19° from the midsemispan to the tip, and trailing-edge sweep of 32.51°. Thickness ratio varied linearly from 0.083 at the wing root to 0.060 at the midsemispan and remained constant to the wing tip. The airfoil sections of the wing were NACA 65A-series sections perpendicular to the quarter-chord line of the wing without the extended inboard leading edge.

The wing was cambered by using linear theory for a lift coefficient of 0.4. Inboard camber lines were calculated for a trapezoidal chordwise loading by the method of reference 3 for a Mach number of 1.2. The camber lines in the vicinity of the wing leading-edge sweep discontinuity and on the outboard portion of the wing were obtained by using Mach 1.0 theory for trapezoidal chordwise loadings on the inboard portion, changing gradually to rectangular chordwise loadings at the wing midsemispan, and remaining rectangular to the wing tip. Some examples of the basic camber lines and the chordwise and spanwise load distributions for which they were calculated are shown in figure 5. The final camber lines are shown in figure 6. These camber lines resulted when the basic camber lines, corrected for aeroelastic wing twist due to the expected aerodynamic loads, were faired together in the chordwise and spanwise directions to form a smooth camber surface.

Streamwise fences which were located at the midsemispan on the upper surface of the wing are shown in figures 7 and 8.

Body.- A complete sketch of the body is given in figure 2. The nose of the model was a surface of revolution with an elliptical meridian profile. Its axis of revolution was alined with the center line of the main body section which was a circular cylinder. The maximum diameter of the nose section was equal to the diameter of the cylindrical section at their junction. Nose coordinates are also shown in figure 2. The rearward portion of the body from 78 percent of the body length to the base (the rearward 35.56 cm (14.00 in.)) was boattailed as shown in figure 3.

Horizontal and vertical tails.- The horizontal tail had an aspect ratio of 4.0, a taper ratio of 0.3, and a quarter-chord-line sweepback angle of 40°. Horizontal-tail incidence was 2°. The vertical tail had an aspect ratio of 1.25, a taper ratio of 0.3, and a quarter-chord-line sweepback angle of 40°. Both horizontal and vertical tails had NACA 65A006 airfoil sections in the streamwise direction. Tail dimensions are given in the model sketch. (See fig. 2.)

Apparatus

The model was tested in the Langley 16-foot transonic tunnel which has a slotted octagonal test section and is operated at atmospheric stagnation pressures. A description of the tunnel is contained in reference 4. The model was sting mounted on a support strut which changed angle of attack in a manner such that the model was kept close to the tunnel center line.

Forces and moments on the model were measured by an internally placed six-component strain-gage balance. Model angle of attack was measured with a pendulum-type strain-gage inclinometer mounted in the model nose. An average model base pressure was obtained from three manifolded pressure taps on the sting inside the model base.

TESTS

All model configurations were tested with fixed boundary-layer transition on the wings and body. The boundary-layer trip on the wing was placed at the 2.5-percent-chord location on both upper and lower surfaces. Transition was fixed around the nose of the model at 2.5 percent of the body length. The roughness strips were 0.1 inch wide and consisted of No. 180 silicon carbide grit particles.

The Mach number was varied from 0.40 to 1.00 and the angle of attack was in the range -5° to 15°. Maximum angle of attack attainable for each configuration at the various Mach numbers was dependent on the balance load limits. Reynolds number based on the reference chord varied from 1.9×10^6 to 3.1×10^6.

The model was tested with and without horizontal (at 2^{o} incidence) and vertical tails. The configuration with the horizontal and vertical tails was tested with and without wing fences at the midsemispan. In addition, body-alone pitch and drag data were obtained.

CORRECTIONS AND ACCURACY

The force data presented herein are adjusted to the condition of free-stream static pressure at the model base. Values of the base pressure coefficient for the various model configurations are presented in figure 9.

The accuracy of the data based on instrument error is estimated to be within the following limits:

M	±0.01
α, deg	±0.1
C_L	
At M = 0.40	±0.028
At M = 0.80	±0.009
C_D at $C_L = 0$	
At M = 0.40	±0.0018
At M = 0.80	±0.0006
C_m	
At M = 0.40	±0.0080
At M = 0.80	±0.0027

RESULTS AND DISCUSSION

The basic aerodynamic characteristics of the wing-body combination are presented in figure 10. In general, differences in wing or body geometry prevent direct comparison of aerodynamic performance with other wing-body combinations. However, some indications of performance can be inferred from indirect comparisons. The data for two comparison configurations are presented in reference 1. The data for the third configuration were obtained during the tests of reference 1 and are unpublished. Sketches of the three configurations are shown at the top of figure 11 along with a sketch of the present wing-body combination. For simplicity, the four wing-body combinations have been given letter designations in figure 11 and are referred to by these designations hereafter.

Configuration A is the wing-body combination of the present investigation and its components have been previously described. Configuration B (data unpublished) consisted of the basic aspect-ratio-8.0 wing with the large inboard leading-edge extensions

and the modified contoured body of reference 1. The inboard wing sections of configuration B had straight camber lines, forward of, and tangent to the original calculated sonic camber lines at maximum section thickness. Configurations C and D, reported in reference 1, consisted of a basic aspect-ratio-8.0 wing combined with cylindrical and modified contoured bodies, respectively.

Drag Due To Lift

The drag-due-to-lift factor k_M for each configuration has been determined from a fit of the equation

$$C_D = C_{D,M} + k_M \left(C_L - C_{L,M}\right)^2$$

to the lift-drag polars. The resulting drag-due-to-lift factors are presented in figure 11 in product form as $k_M A$. It should be noted that $k_M A$ is independent of the wing reference area used in calculating the two parameters of the product. Also presented in figure 11 are the conditions for zero suction, A/C_{L_α}, and 100-percent suction, $1/\pi$.

Comparison of the parameter $k_M A$ for configuration A with that of configuration B, which had a similar wing planform, shows that configuration A had lower drag due to lift at Mach numbers from about 0.80 to 0.90. (See fig. 11.) Above a Mach number of 0.90, configuration B appears to have lower drag due to lift. However, the models are not directly comparable because configuration A has a cylindrical body and configuration B has a modified contoured body. It is probable that the cylindrical body causes configuration A to have larger values of $k_M A$ at high subsonic speeds. Evidence of such a body effect is shown in figure 11 where a decrease of 10 percent in $k_M A$ at a Mach number of 0.92 is obtained by going from a cylindrical body (configuration C) to a modified contoured body (configuration D). The effect on drag due to lift of a small difference in leading-edge Reynolds number between configurations A and B has been assumed to be negligible on the basis of results presented in reference 5.

The largest effect on $k_M A$ shown in figure 11 is due to the addition of inboard leading-edge extensions to the wing of reference 1. (Compare configurations B and D.) The leading-edge extensions delayed the abrupt increase in $k_M A$ with Mach number that occurred on the basic wing by about 0.05 in Mach number.

Maximum Lift-Drag Ratio

The variations of adjusted and unadjusted maximum lift-drag ratios for configurations A and B are shown in figure 12. In order to compare these two configurations, which had similar wing planforms, it was necessary to adjust the drag-coefficient data of configuration A for body size and Reynolds number and the lift-drag polars of

configuration B for body shape. These adjustments were required so that the influence of the different bodies on maximum lift-drag ratio could be minimized. Body-alone basic data are presented in figure 13 and a comparison with the cylindrical body of reference 2 is shown in figure 14. (About 0.0015 of the difference in body drag coefficient shown in figure 14 can be attributed to skin friction.) The body-alone drag was subtracted from the total drag of configuration A and the resulting increment was corrected to the Reynolds number of configuration B. Then, new lift-drag polars were obtained by adding the drag of the cylindrical body of reference 2 to the corrected drag increment. Configuration B was adjusted to the same cylindrical body by using increments from the basic lift and drag data of configurations C and D. Configuration B could not be adjusted by simple subtraction and addition of body drag because modified contoured body-alone data were not available. No mutual interference effects were considered in the adjustments to the data.

With the data adjusted to conditions representing comparable values of fuselage drag, a comparison of $(L/D)_{max}$ for configurations A and B (fig. 12(b)) indicates that configuration A has a maximum increase in $(L/D)_{max}$ of about 1.0 at a Mach number of 0.86, above that of configuration B.

Flow Visualization

Flow-visualization studies using the fluorescent-oil film method of reference 6 were made on the wings of configurations A and B at a lift coefficient of about 0.36. These studies indicate a substantial difference in the Mach number at which flow separation near the trailing edge of the inboard portions of the wings can first be detected. The first indication of inboard trailing-edge flow separation occurred at a Mach number of 0.86 on the wing of configuration B and at a Mach number of 0.92 on the wing of configuration A. It would appear that the delay in the Mach number at which flow separation occurs near the trailing edge of the inboard portion of the wing can be attributed to the use of supersonic camber lines.

Effect Of Wing Fences

The basic aerodynamic characteristics for the model with and without wing fences and with a horizontal-tail incidence of 2^o are presented in figure 15. Summary data are presented in figure 16 to show the effect of the wing fences on the longitudinal aerodynamic characteristics of the model.

In general, the wing fences increased lift-curve slope slightly (measured at $\alpha = 0^o$) at most Mach numbers (fig. 16(c)). The wing fences increased drag coefficient at all Mach numbers below 1.00 (figs. 15(b) and 16(a)). The increase in drag coefficient due to the wing fences is reflected in the maximum lift-drag ratio (untrimmed) which was

decreased by about 1.00 at Mach numbers from 0.70 to 0.94 (fig. 16(b)). At Mach number 1.00 there was no effect of wing fences on maximum lift-drag ratio.

The most pronounced effect of wing fences was on the pitching-moment curves which, in general, were made more linear particularly at high lift coefficients (fig. 15(c)). The slopes of the pitching-moment curves $C_{m_{C_L}}$ at low lift coefficients were only slightly affected by the presence of the wing fences (figs. 15(c) and 16(c)).

CONCLUSIONS

The longitudinal aerodynamic characteristics of a model with a wing designed for high efficiency at high subsonic speeds have been determined at Mach numbers from 0.40 to 1.00. The wing had a leading-edge sweep discontinuity at the midsemispan and was cambered for a lift coefficient of 0.4. The model and components were tested in the following combinations: wing, body, tails, and wing fences; wing, body, and tails; wing and body; and body alone. The test results indicate the following:

1. The wing-body combination had lower drag due to lift than a similar wing-body combination at Mach numbers from 0.80 to 0.90.

2. Streamwise wing fences located at the wing leading-edge discontinuity (for the wing-body-tail combination) increased drag coefficient, decreased maximum untrimmed lift-drag ratio at all Mach numbers below 1.00, and reduced the nonlinearity of the pitching-moment curves at high lift coefficients.

Langley Research Center,
National Aeronautics and Space Administration,
Langley Station, Hampton, Va., January 15, 1966.

REFERENCES

1. Heath, Atwood R., Jr.: Longitudinal Aerodynamic Characteristics of a High-Subsonic-Speed Transport Airplane Model With a Cambered 40° Sweptback Wing of Aspect Ratio 8 at Mach Numbers to 0.96. NASA TN D-218, 1960.

2. Re, Richard J.: Aerodynamic Effects of Modifying Wing Inboard Trailing-Edge Camber of a Model at High Subsonic Speeds. NASA TN D-1809, 1963.

3. Tucker, Warren A.: A Method for the Design of Sweptback Wings Warped To Produce Specified Flight Characteristics at Supersonic Speeds. NACA Rept. 1226, 1955. (Supersedes NACA RM L51F08.)

4. Ward, Vernon G.; Whitcomb, Charles F.; and Pearson, Merwin D.: Air-Flow and Power Characteristics of the Langley 16-Foot Transonic Tunnel With Slotted Test Section. NACA RM L52E01, 1952.

5. Osborne, Robert S.; and Kelly, Thomas C.: A Note on the Drag Due to Lift of Delta Wings at Mach Numbers Up to 2.0. NASA TN D-545, 1960. (Supersedes NACA RM L53A16a.)

6. Loving, Donald L.; and Katzoff, S.: The Fluorescent-Oil Film Method and Other Techniques for Boundary-Layer Flow Visualization. NASA MEMO 3-17-59L, 1959.

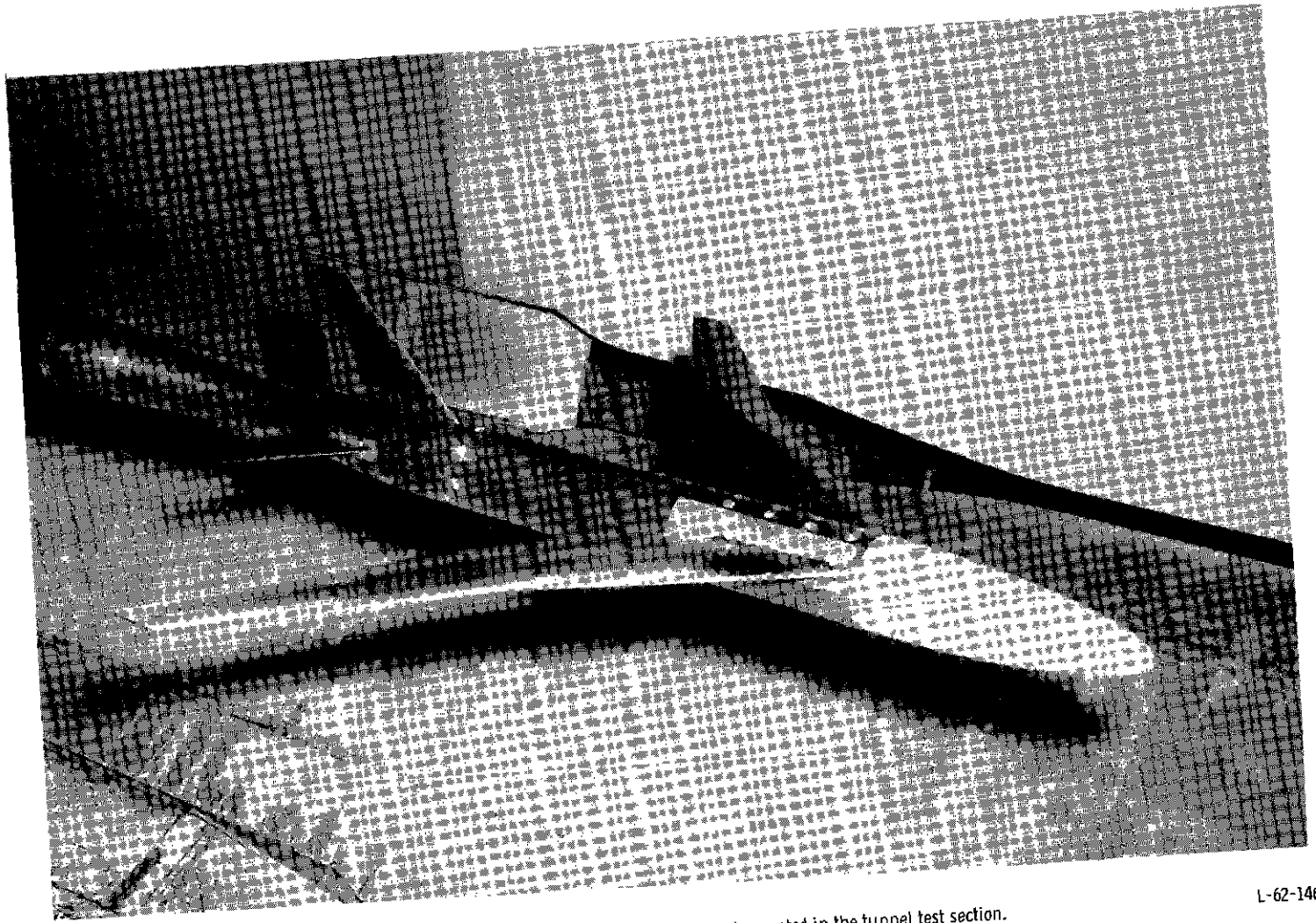

L-62-1460

Figure 1.- Photograph showing complete model mounted in the tunnel test section.

Normalized nose coordinates	
$\frac{x'}{l}$	$\frac{r}{R}$
0	0
.0028	.142
.0085	.244
.0211	.380
.0283	.436
.0424	.528
.0566	.601
.0706	.660
.0847	.713
.0988	.759
.1130	.802
.1694	.918
.2260	.980
.2824	1.000

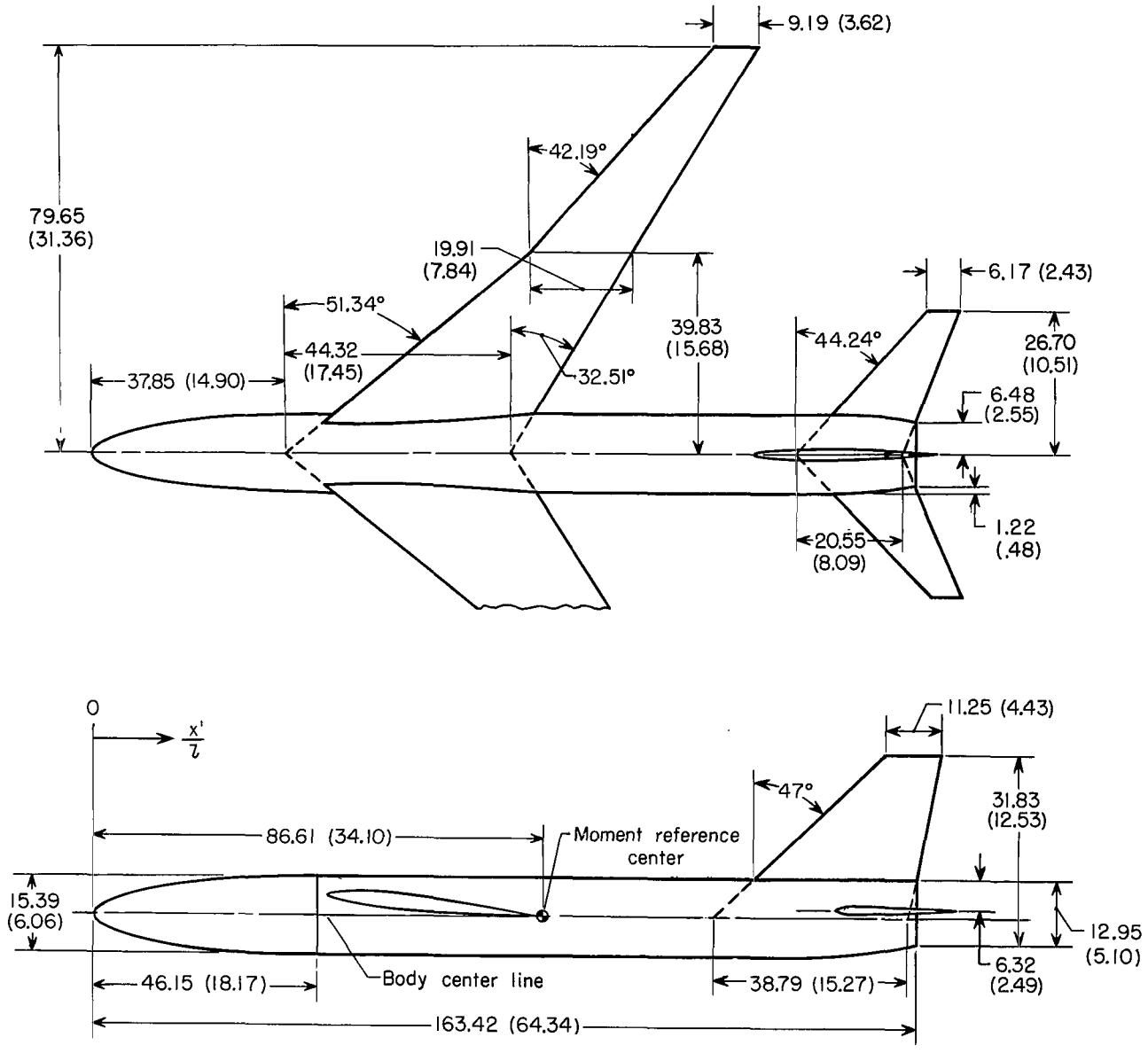

Figure 2.- Sketch of complete model. All linear dimensions are given in centimeters and then in parentheses in inches. All angular dimensions are in degrees.

Normalized afterbody coordinates			
x'/ℓ	r/R	x'/ℓ	r/R
0.7823	1.158	0.9089	1.063
.7981	1.155	.9248	1.033
.8140	1.152	.9406	1.003
.8298	1.145	.9565	.967
.8458	1.135	.9723	.927
.8614	1.122	.9882	.881
.8772	1.106	1.0000	.841
.8931	1.086		

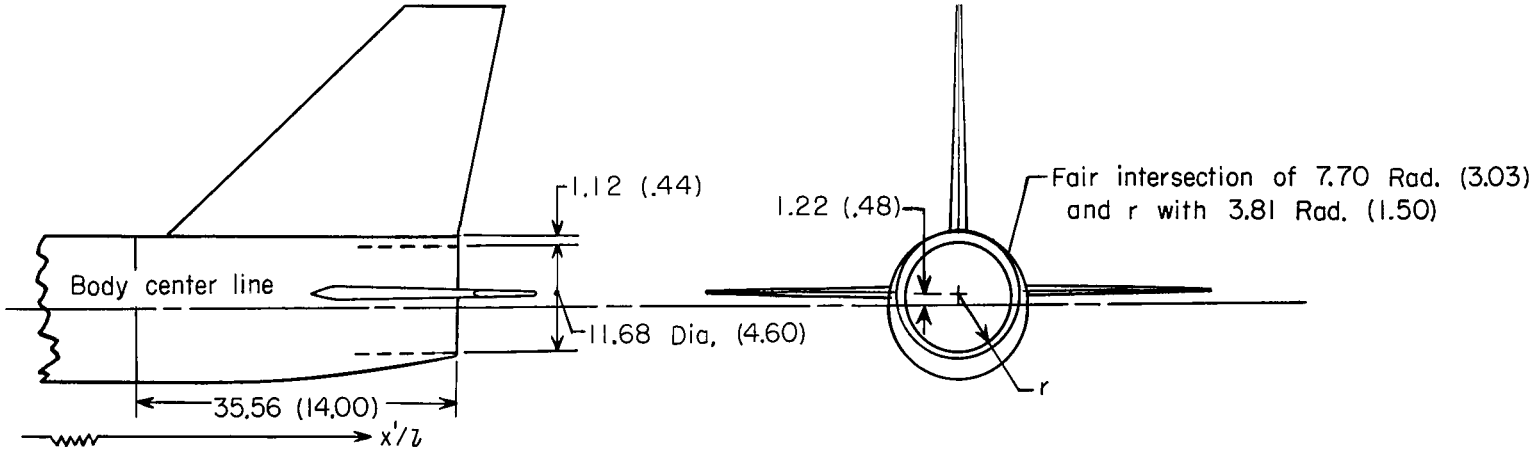

Figure 3.- Sketch showing afterbody boattailing details. All linear dimensions are given in centimeters and then in parentheses in inches.

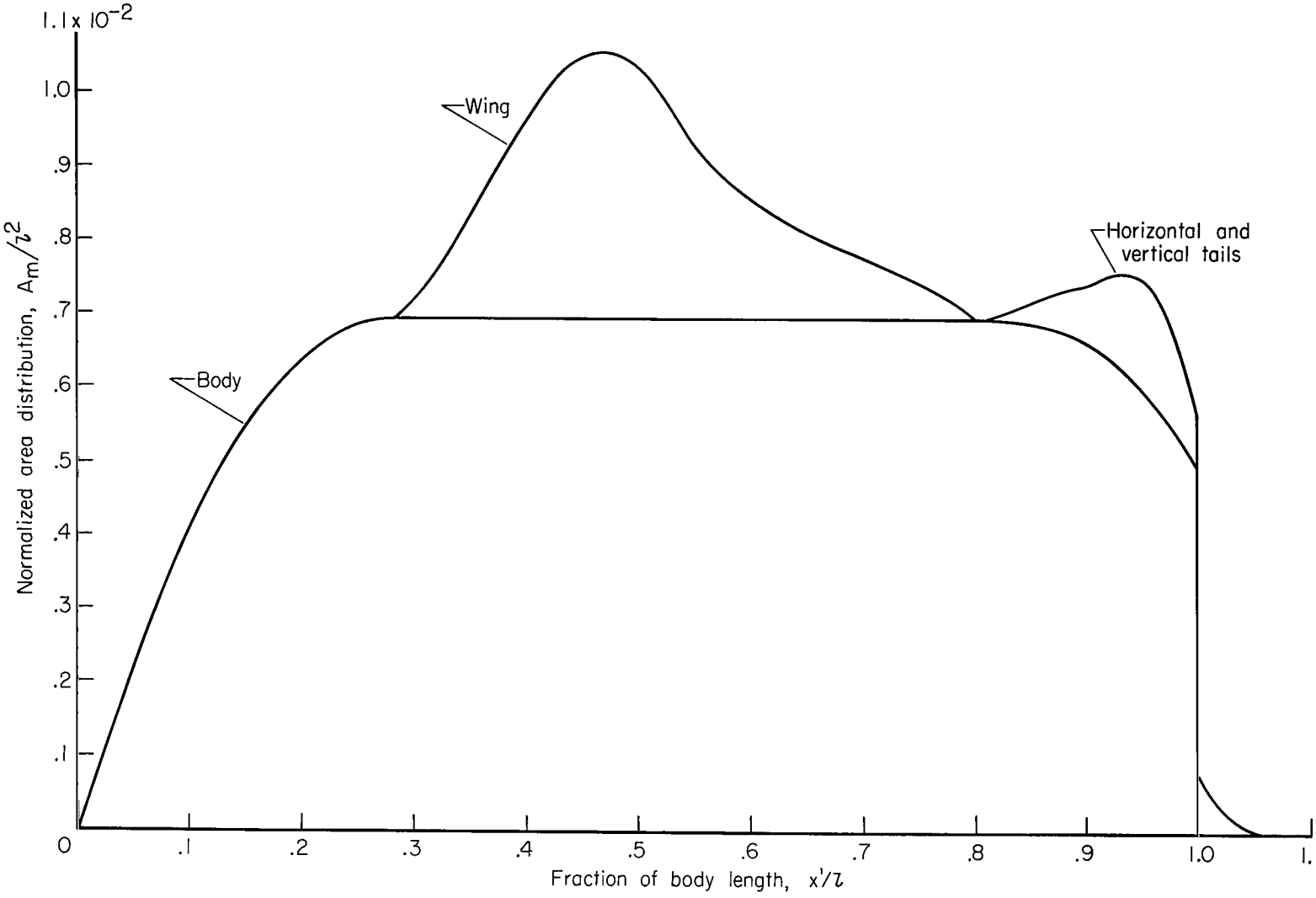

Figure 4.- Normalized cross-sectional-area distribution of the complete model.

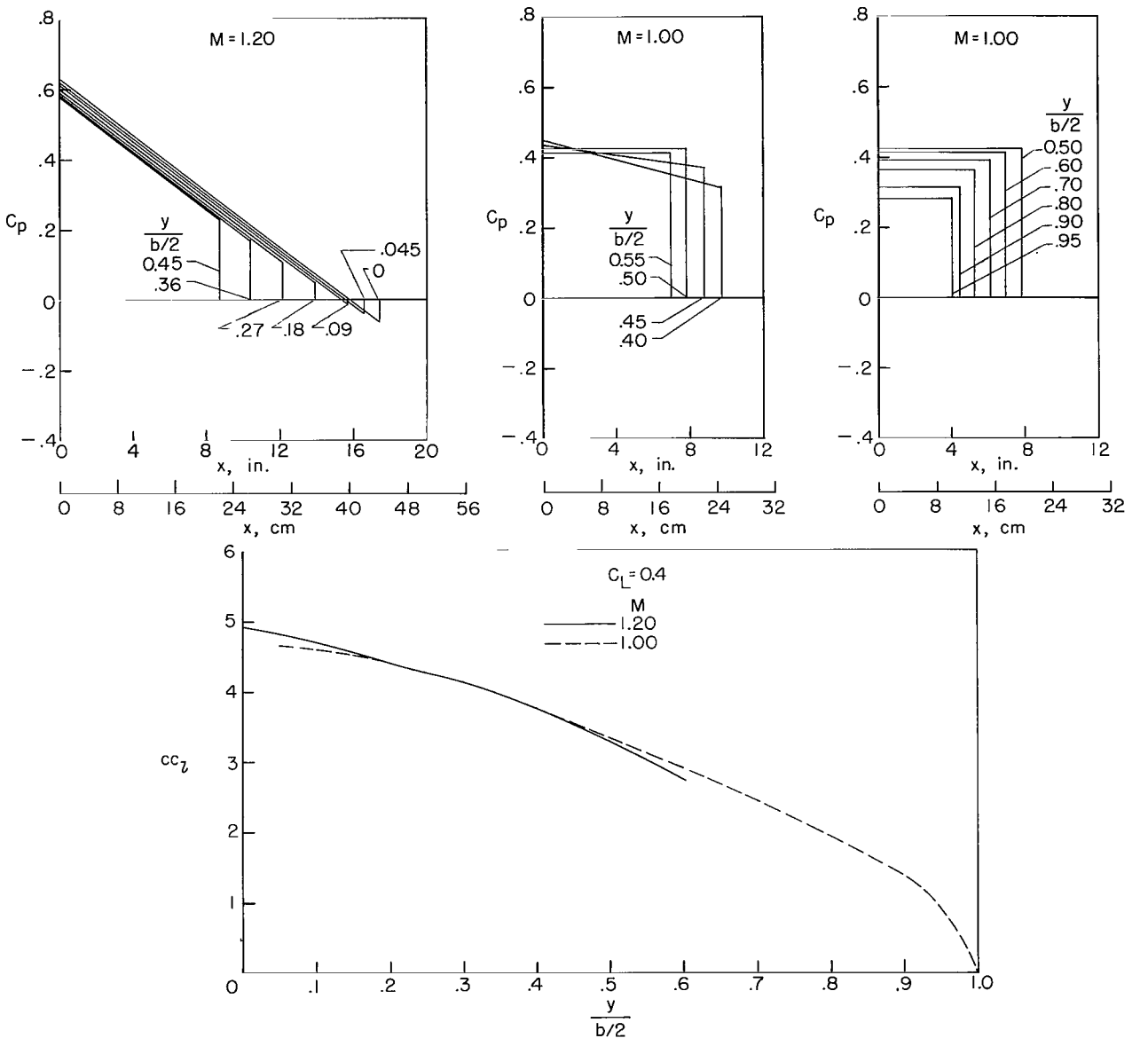

(a) Typical design chordwise pressure distributions and span load distributions.

Figure 5.- Design chordwise pressure distributions, span load distributions, and calculated camber lines.

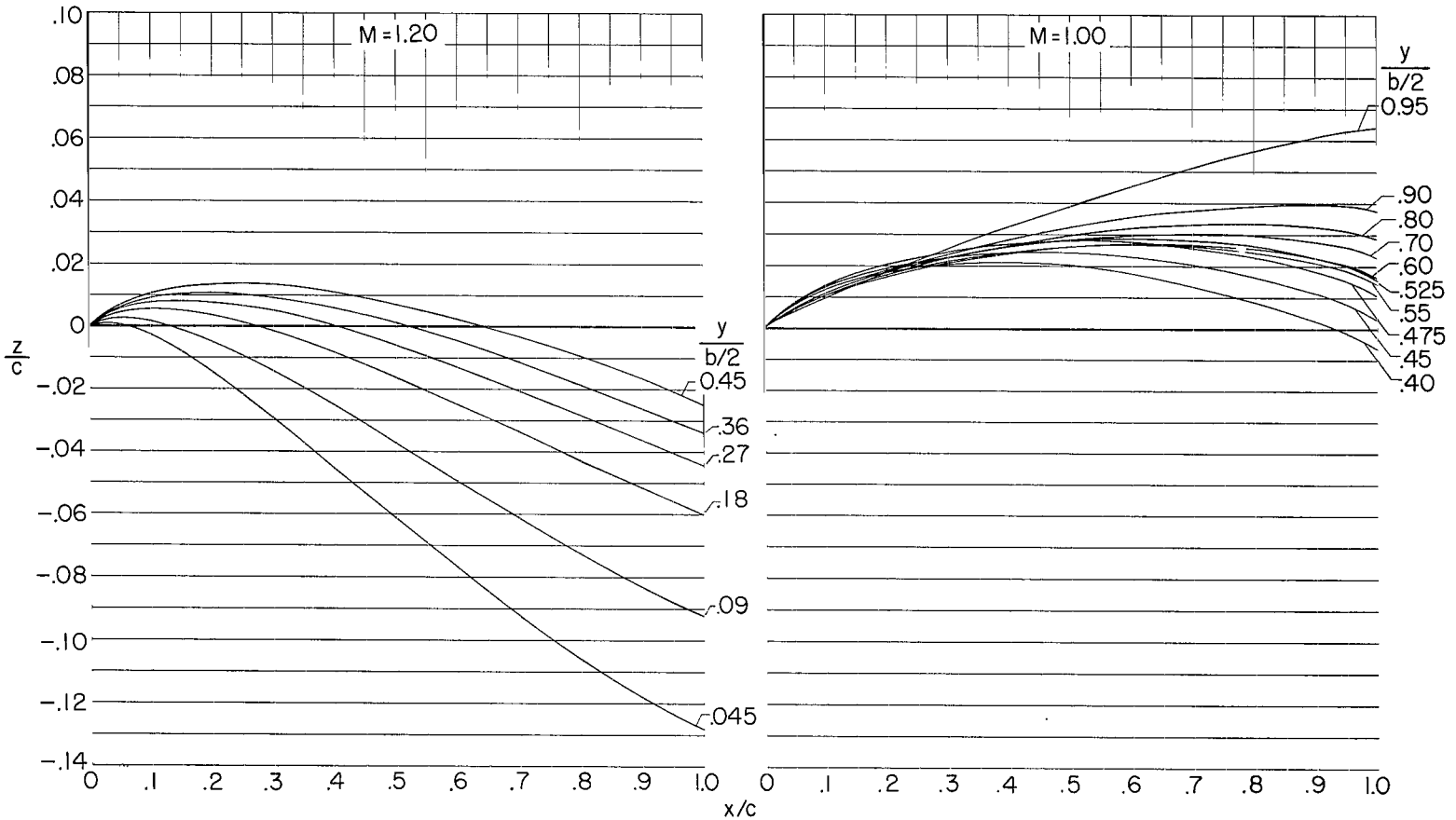

(b) Calculated camber lines.

Figure 5.- Concluded.

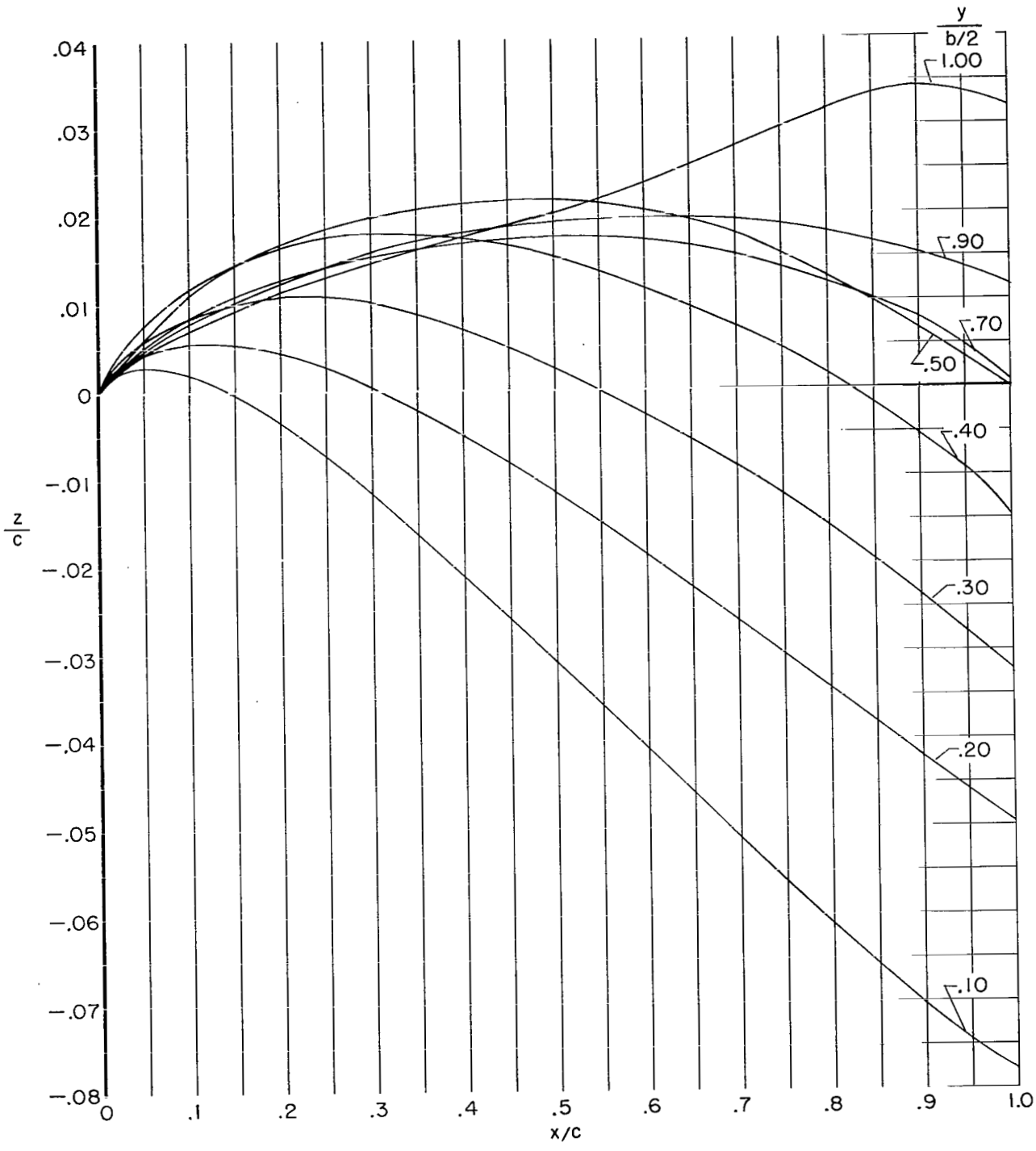

Figure 6.- Final wing camber lines incorporating twist and spanwise and chordwise fairing.

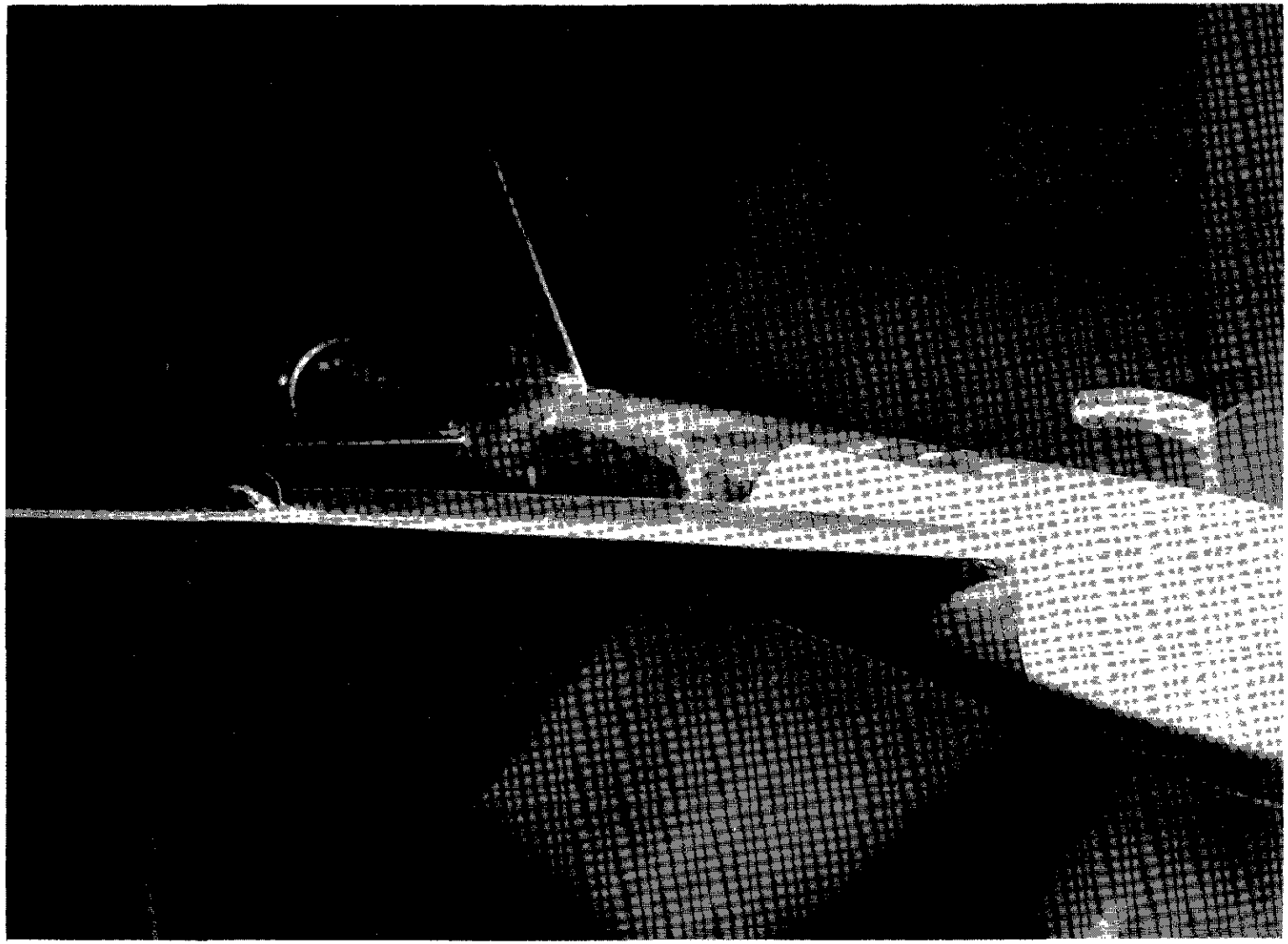

Figure 7.- Photograph of model with wing fences.

L-62-1524

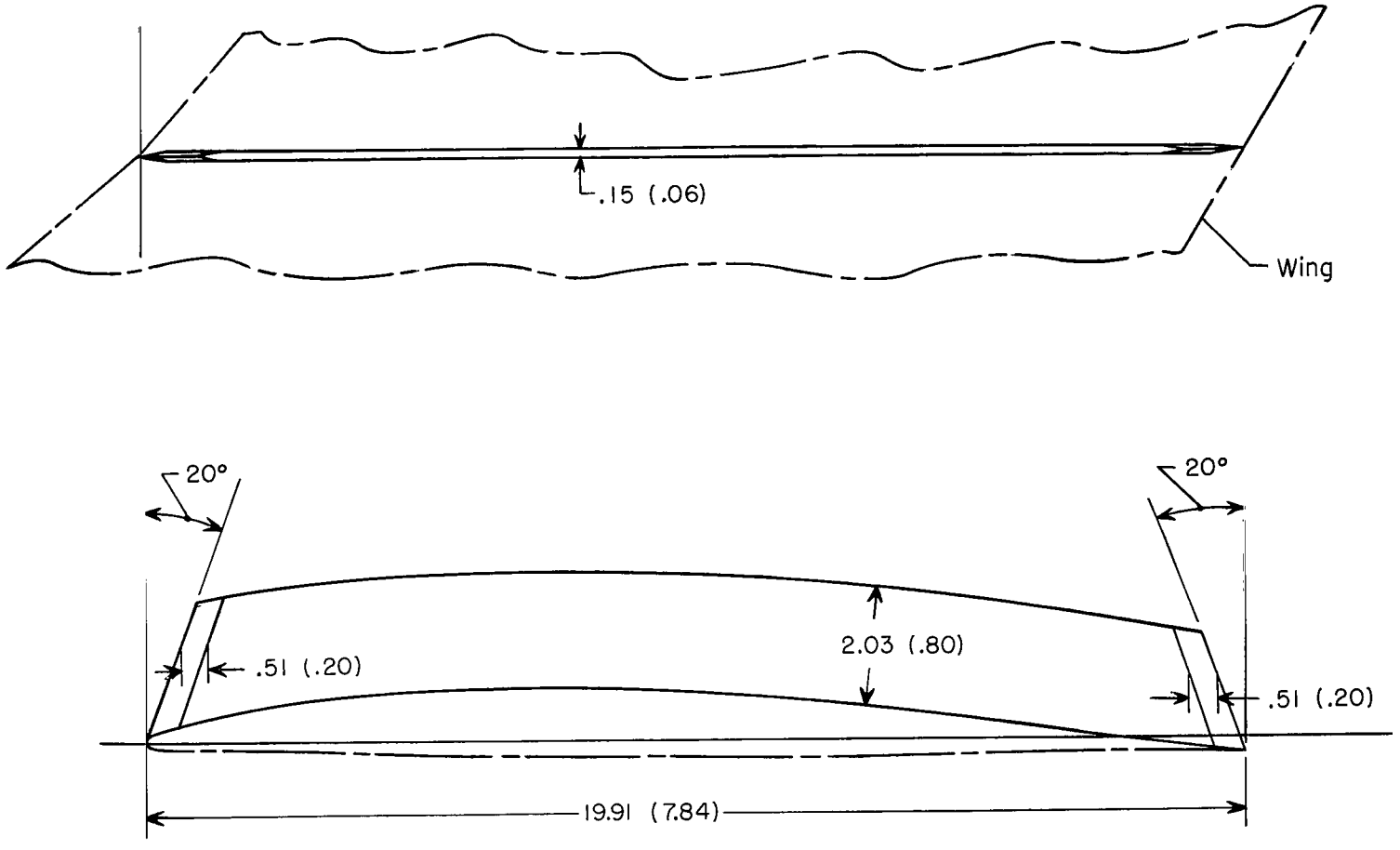

Figure 8.- Sketch of wing fences. All linear dimensions are given in centimeters and then in parentheses in inches. All angular dimensions are in degrees.

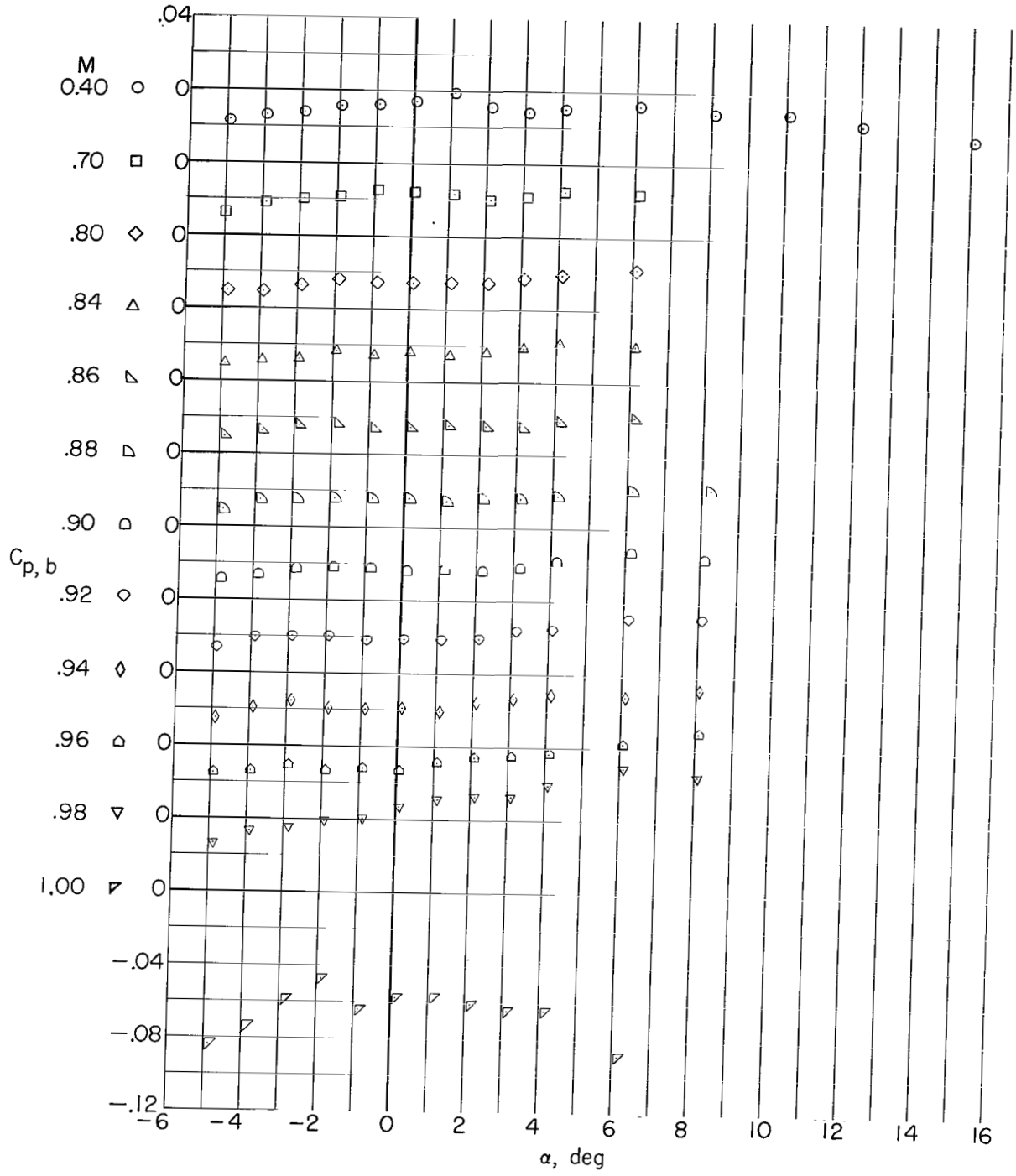

(a) Model without horizontal and vertical tails.

Figure 9.- Base pressure coefficients for the various model configurations.

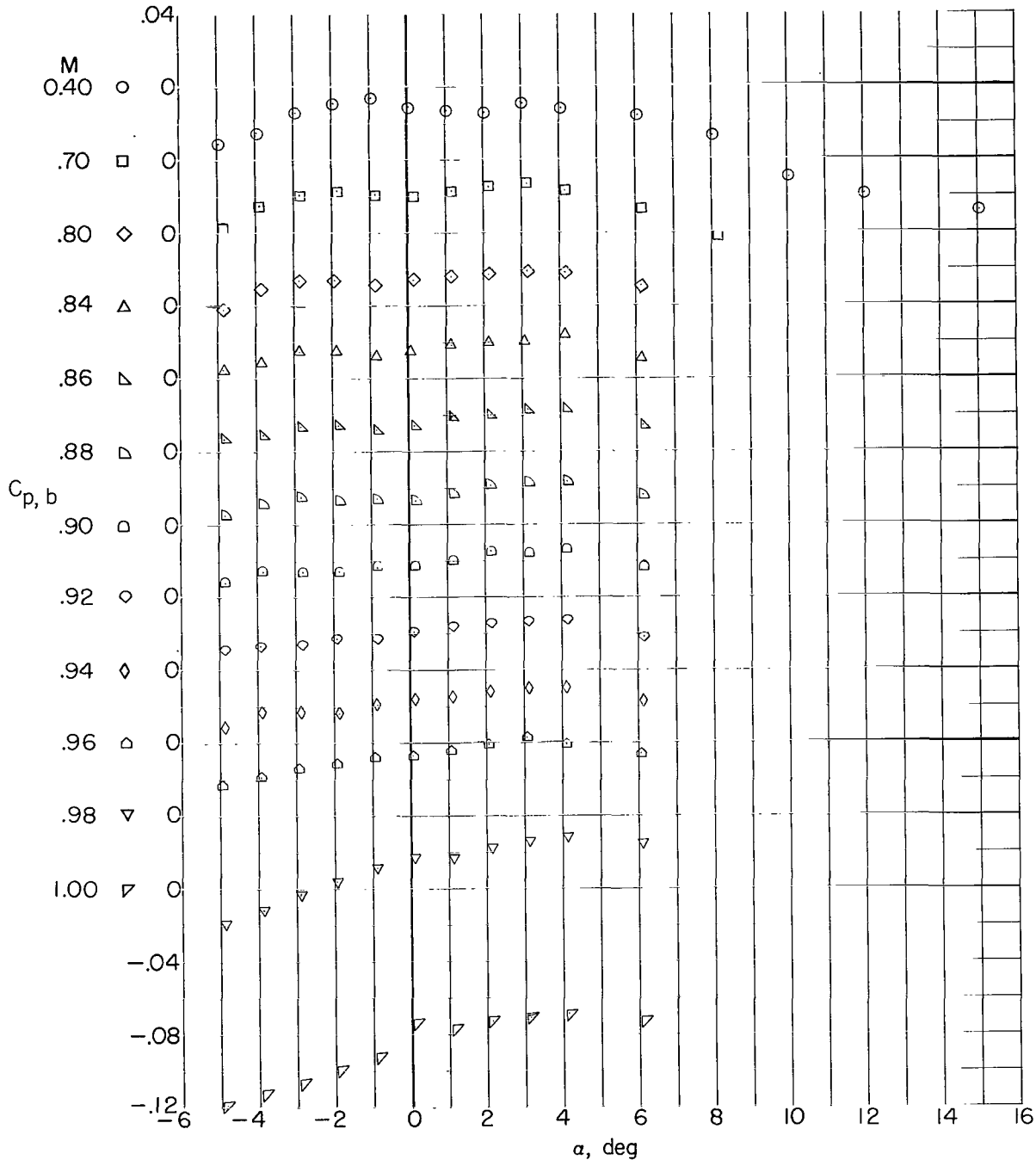

(b) Body alone.

Figure 9.- Continued.

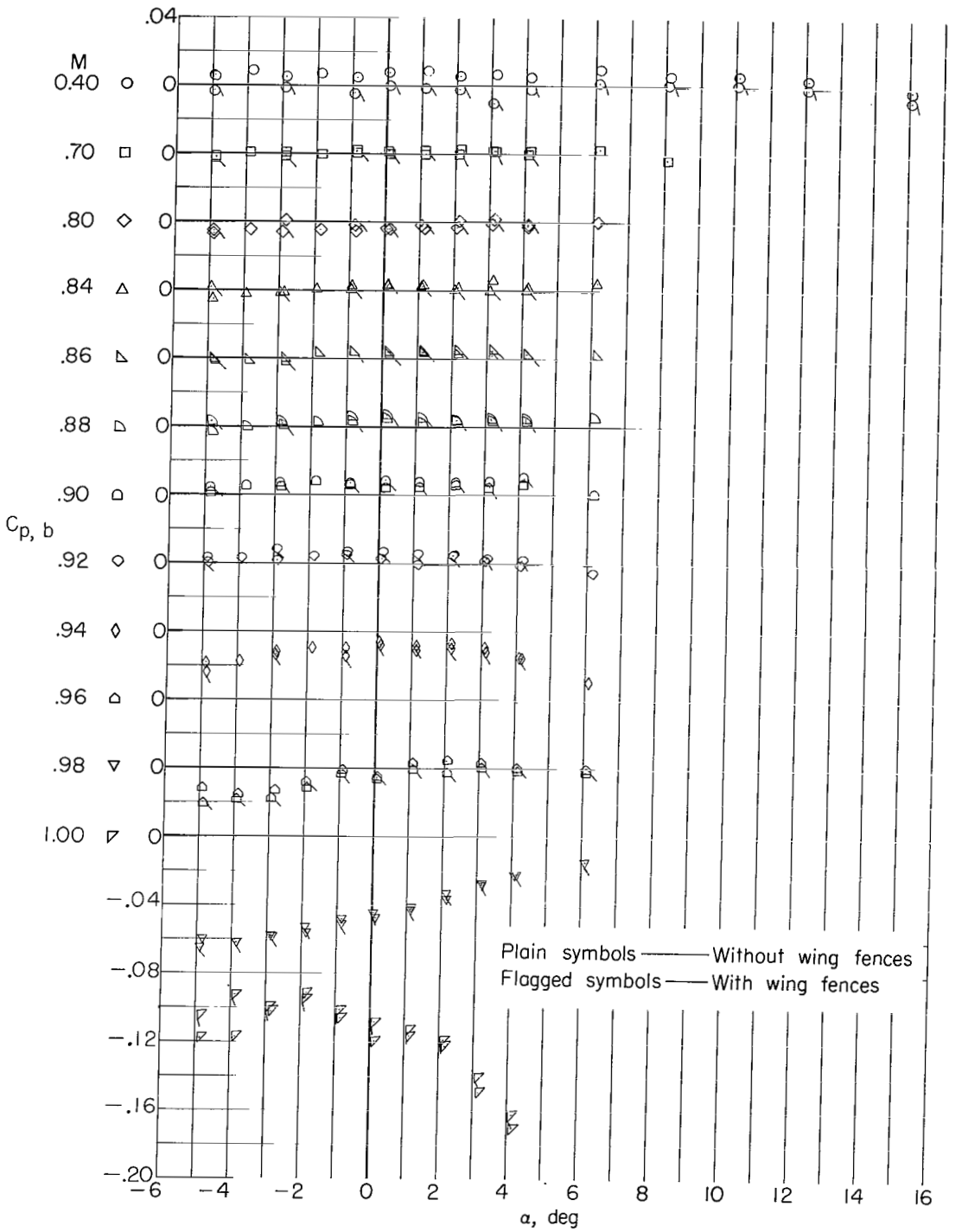

(c) Complete model ($i_t = 2^0$) with and without wing fences.

Figure 9.- Concluded.

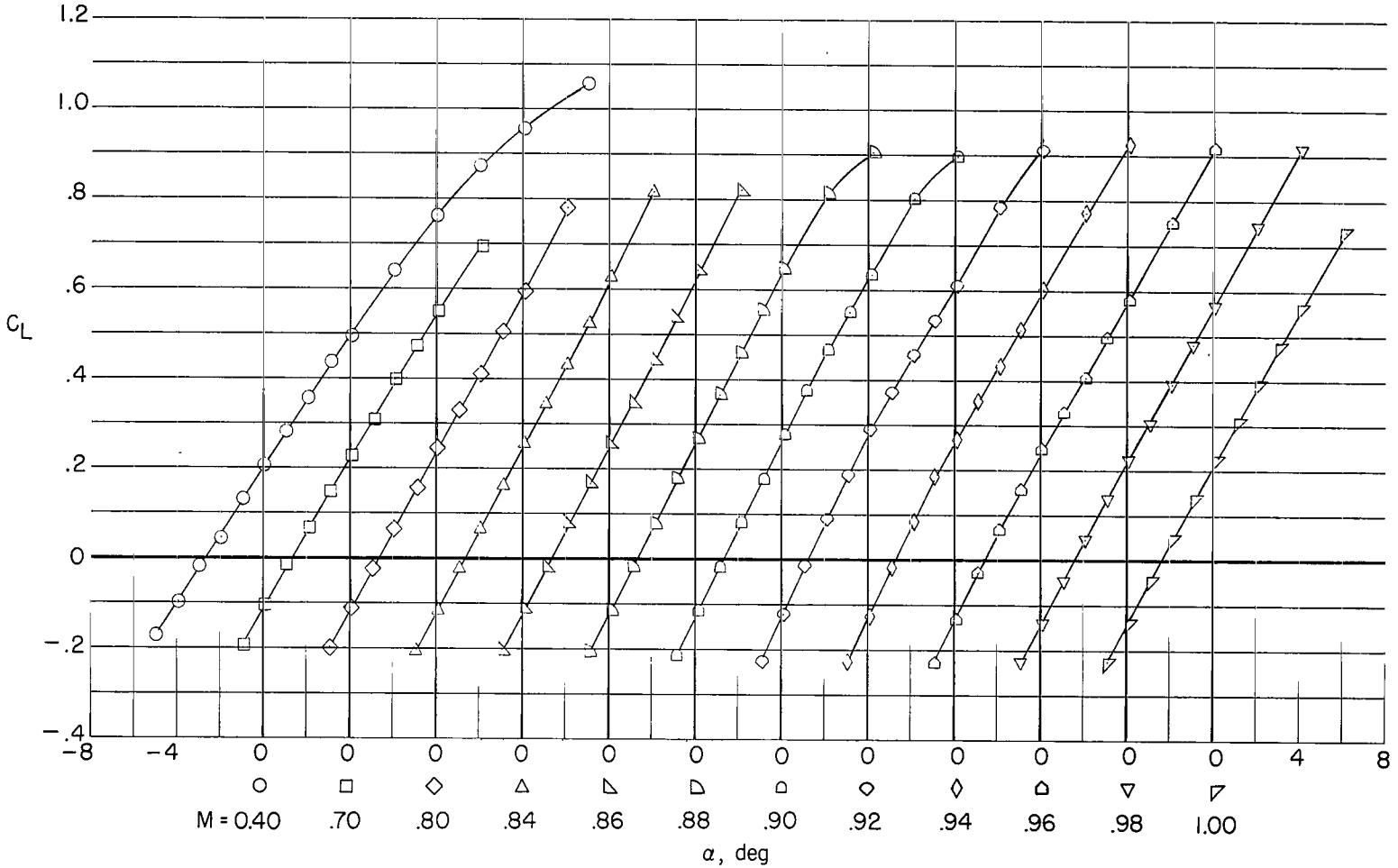

(a) Lift coefficient.

Figure 10.- Longitudinal aerodynamic characteristics of the model without horizontal and vertical tails.

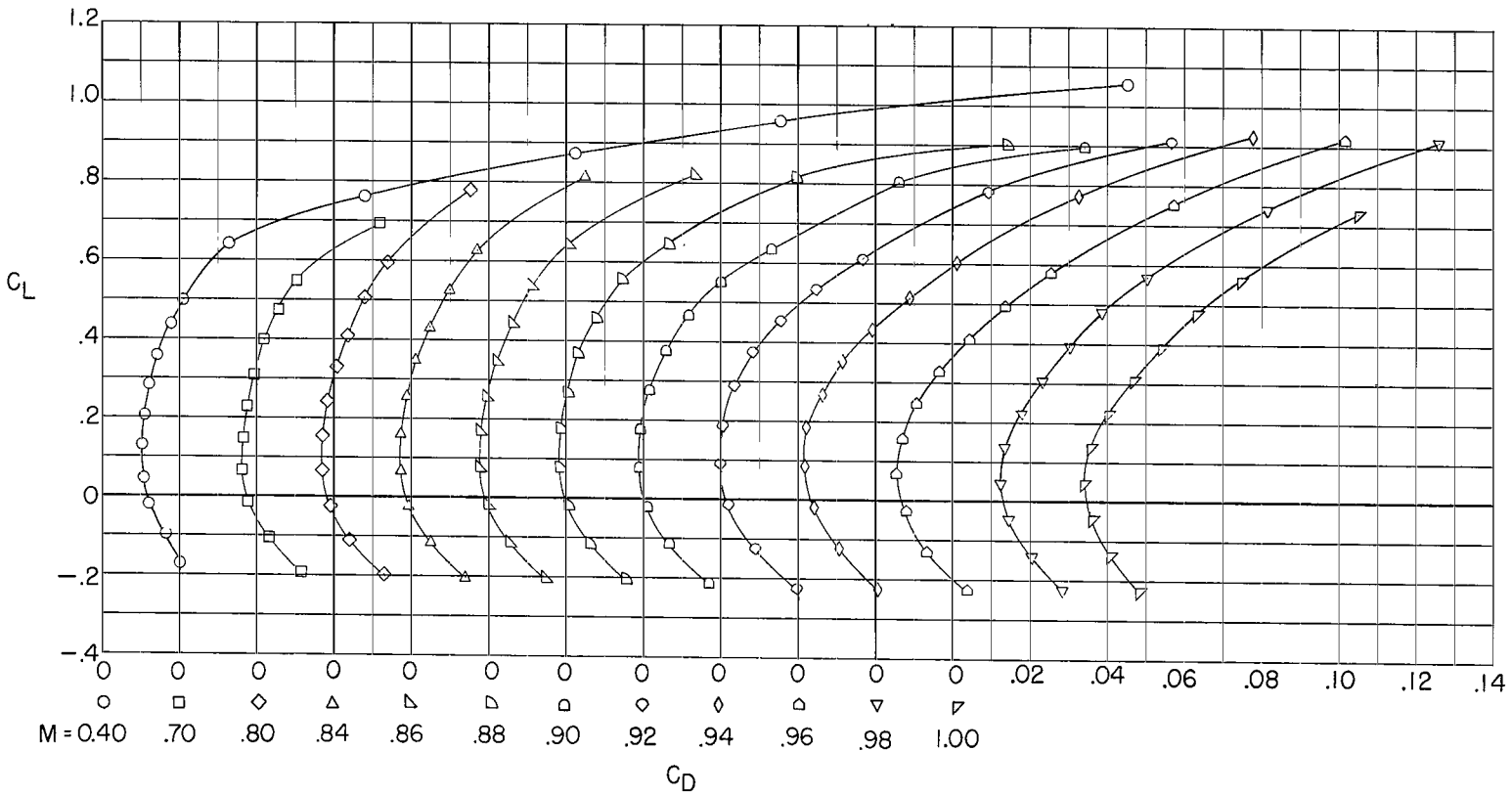

(b) Drag coefficient.

Figure 10.- Continued.

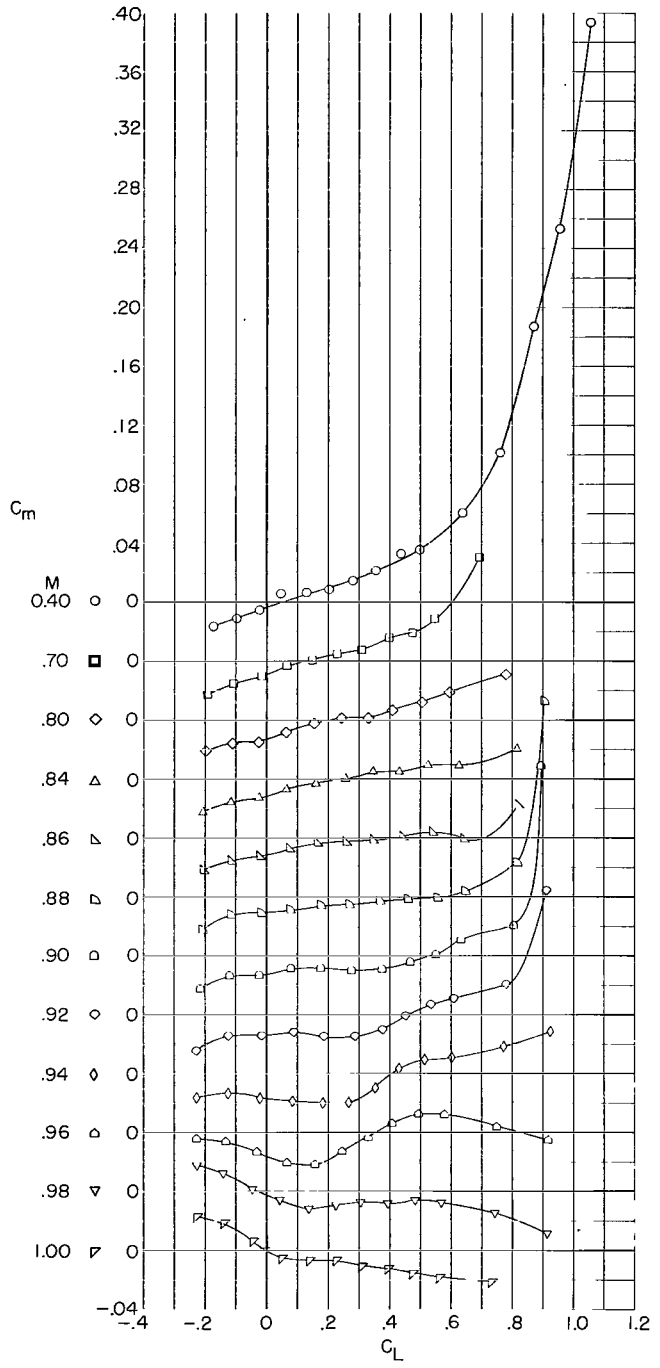

(c) Pitching-moment coefficient.

Figure 10.- Concluded.

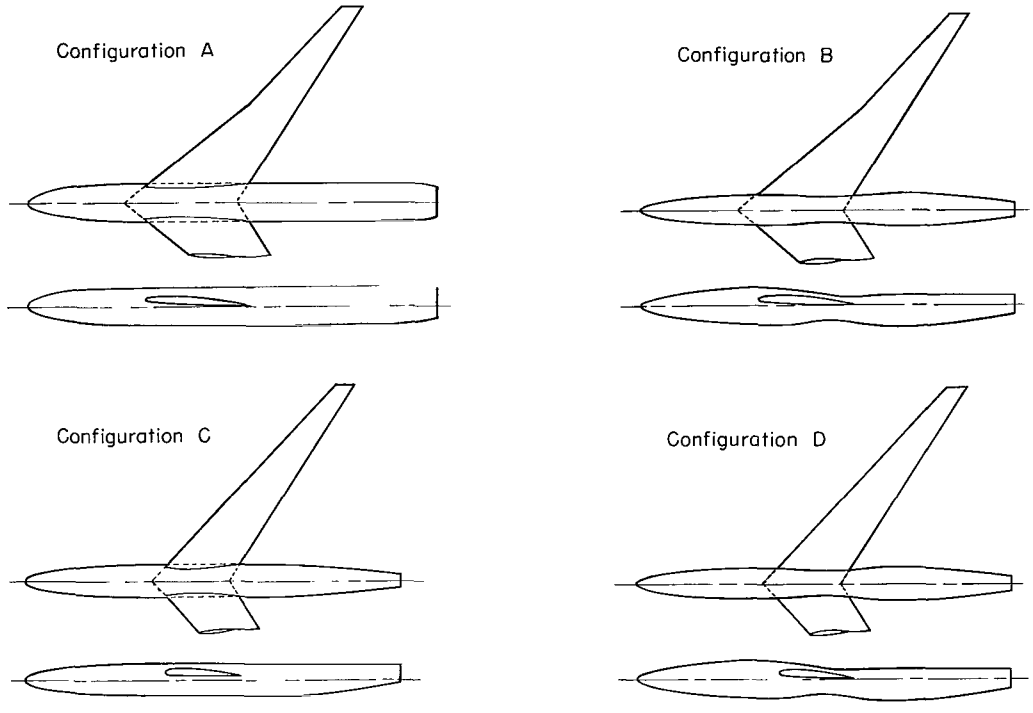

Line code	Configuration	Wing leading-edge sweep $\frac{y}{b/2} < 0.50$	Wing leading-edge sweep $\frac{y}{b/2} > 0.50$	Wing planform aspect ratio	Body shape	Basic data source
———	A	51.34°	42.19°	6.83	Cylindrical	Figure 12(b)
– – – –	B	50.21°	42.19°	6.97	Modified contoured	Unpublished data
——— – ———	C	42.19°	42.19°	8.00	Cylindrical	Reference 1
——— – – ———	D	42.19°	42.19°	8.00	Modified contoured	Reference 1

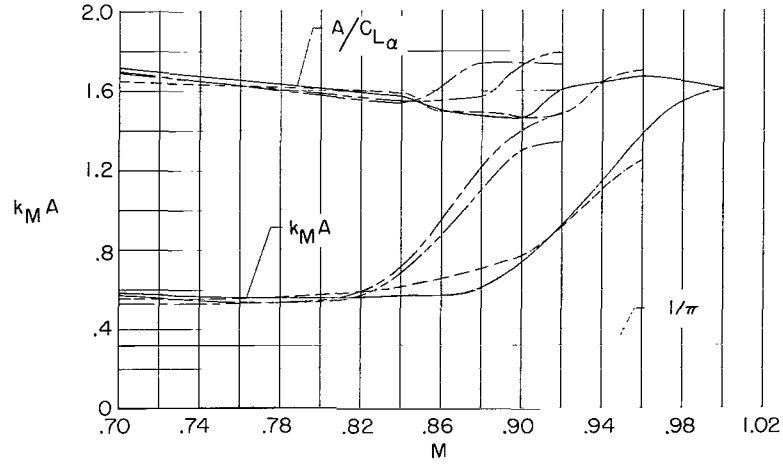

Figure 11.- Variation of drag-due-to-lift parameter $k_M A$ with Mach number for four wing-body combinations having high-aspect-ratio wings.

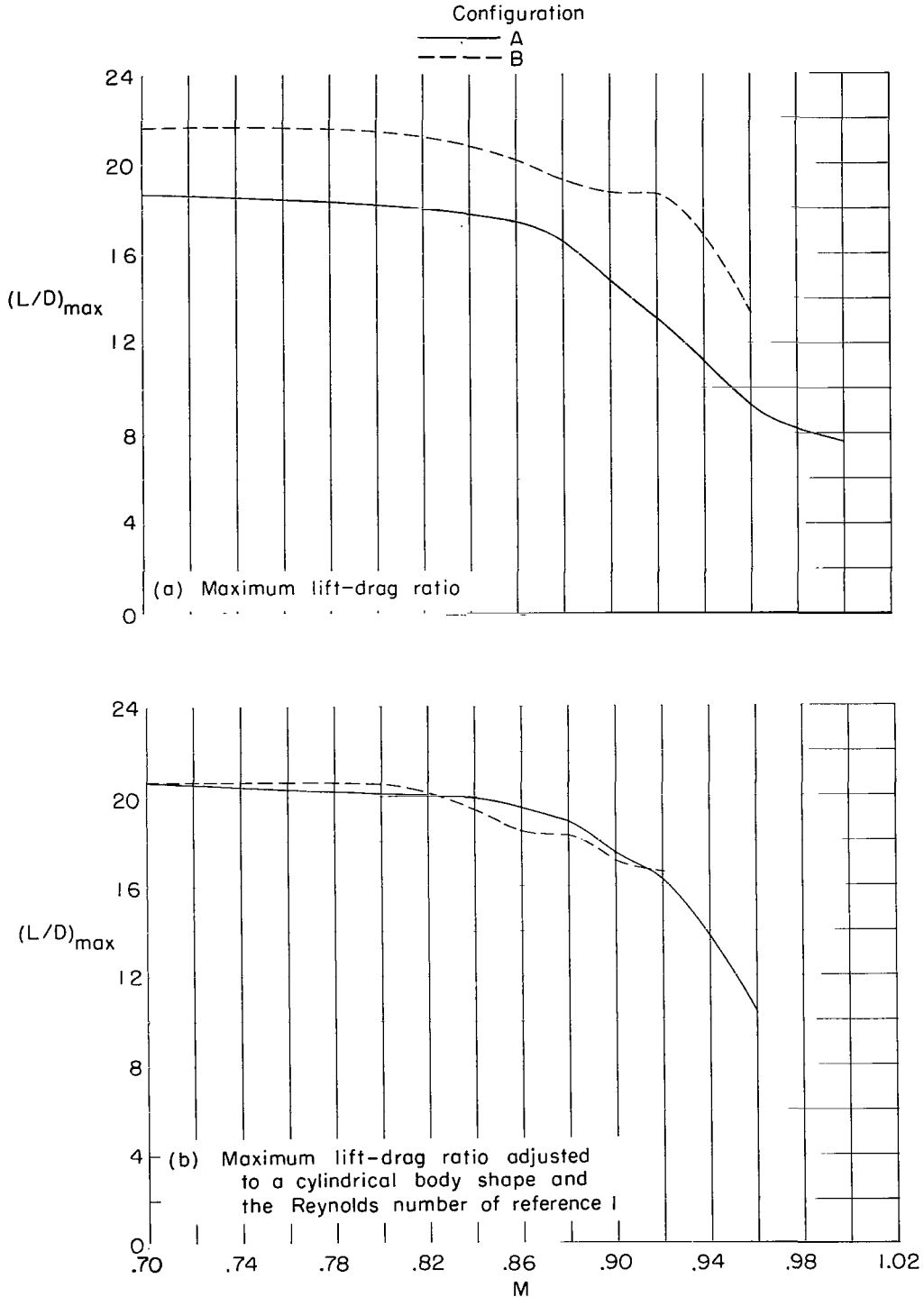

Figure 12.- Variation of maximum lift-drag ratio with Mach number for the wing-body combination of the present investigation (configuration A) and a similar wing-body combination (configuration B) with and without adjustments for differences in body shape and Reynolds number.

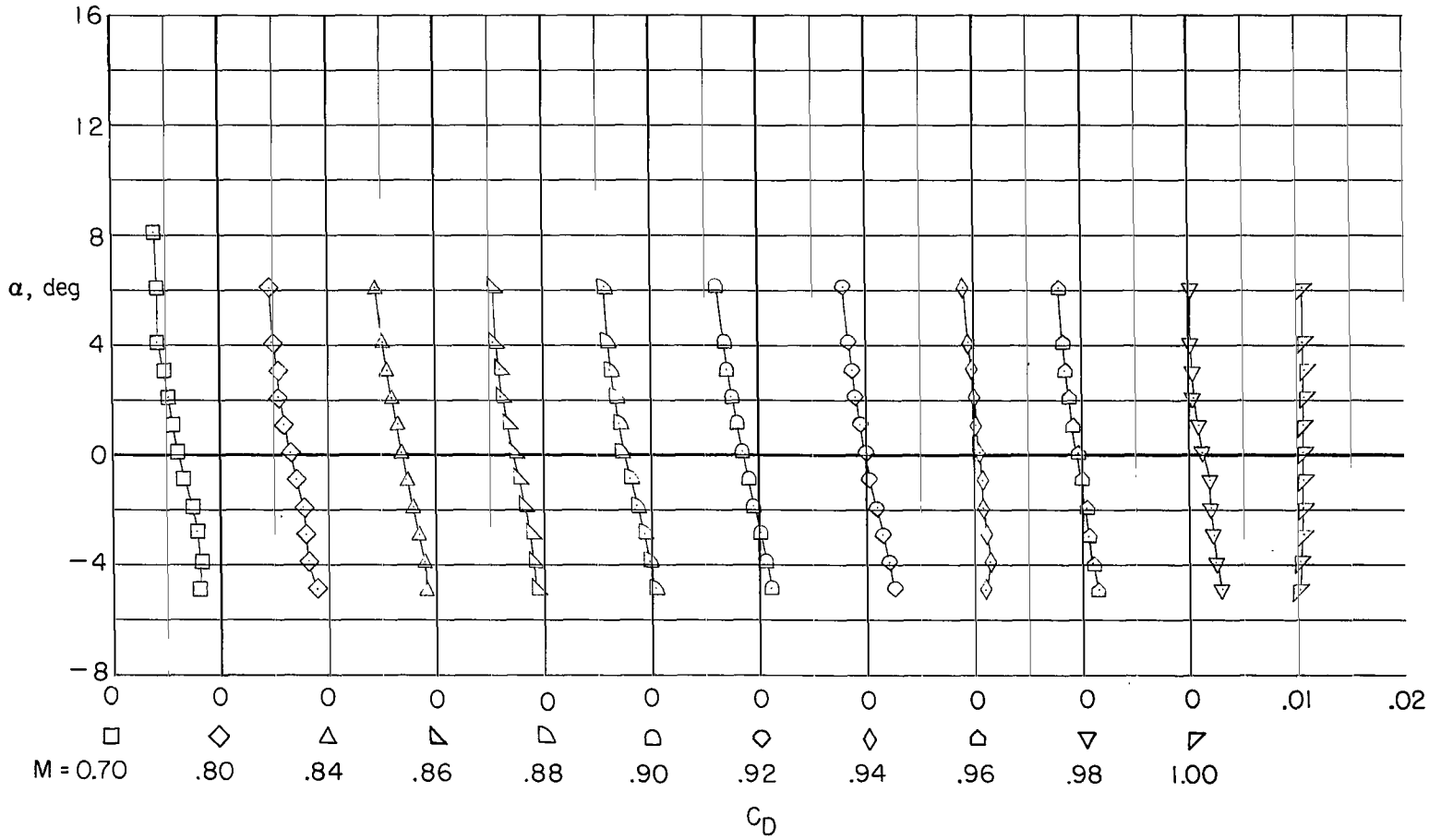

(a) Drag coefficient.

Figure 13.- Drag and pitching-moment characteristics of the body alone.

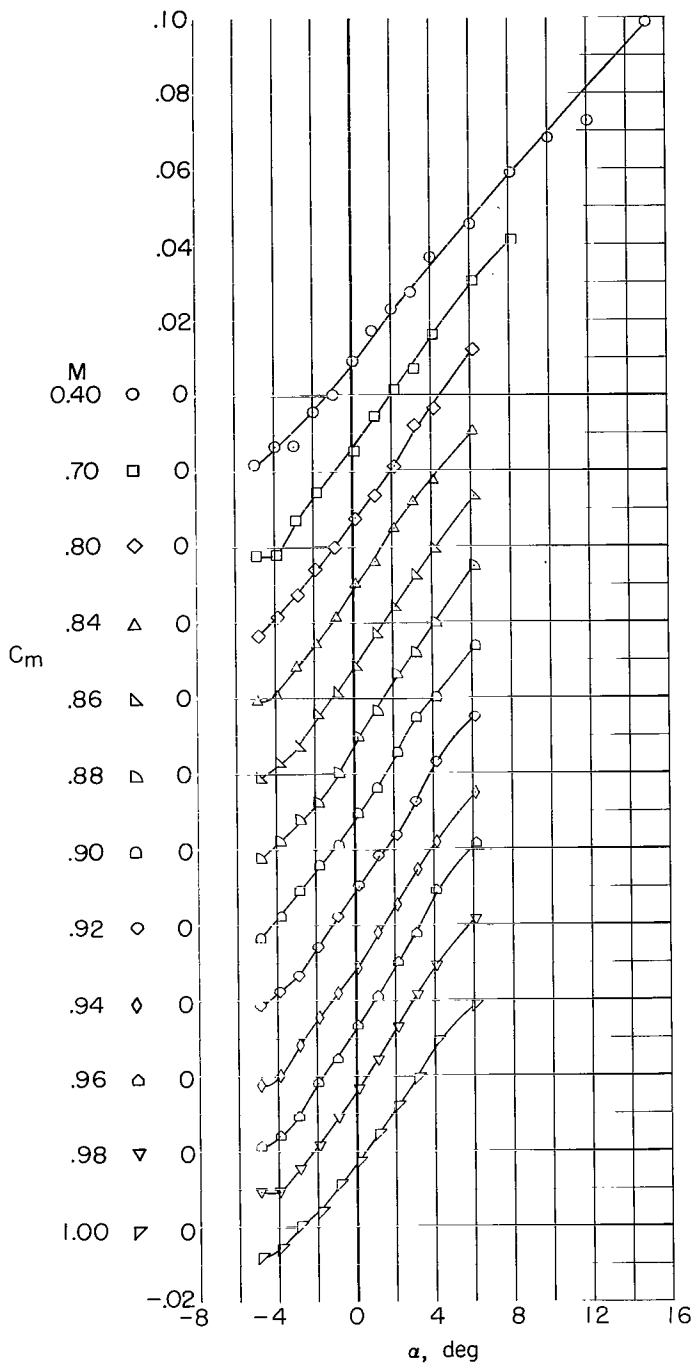

(b) Pitching-moment coefficient.

Figure 13.- Concluded.

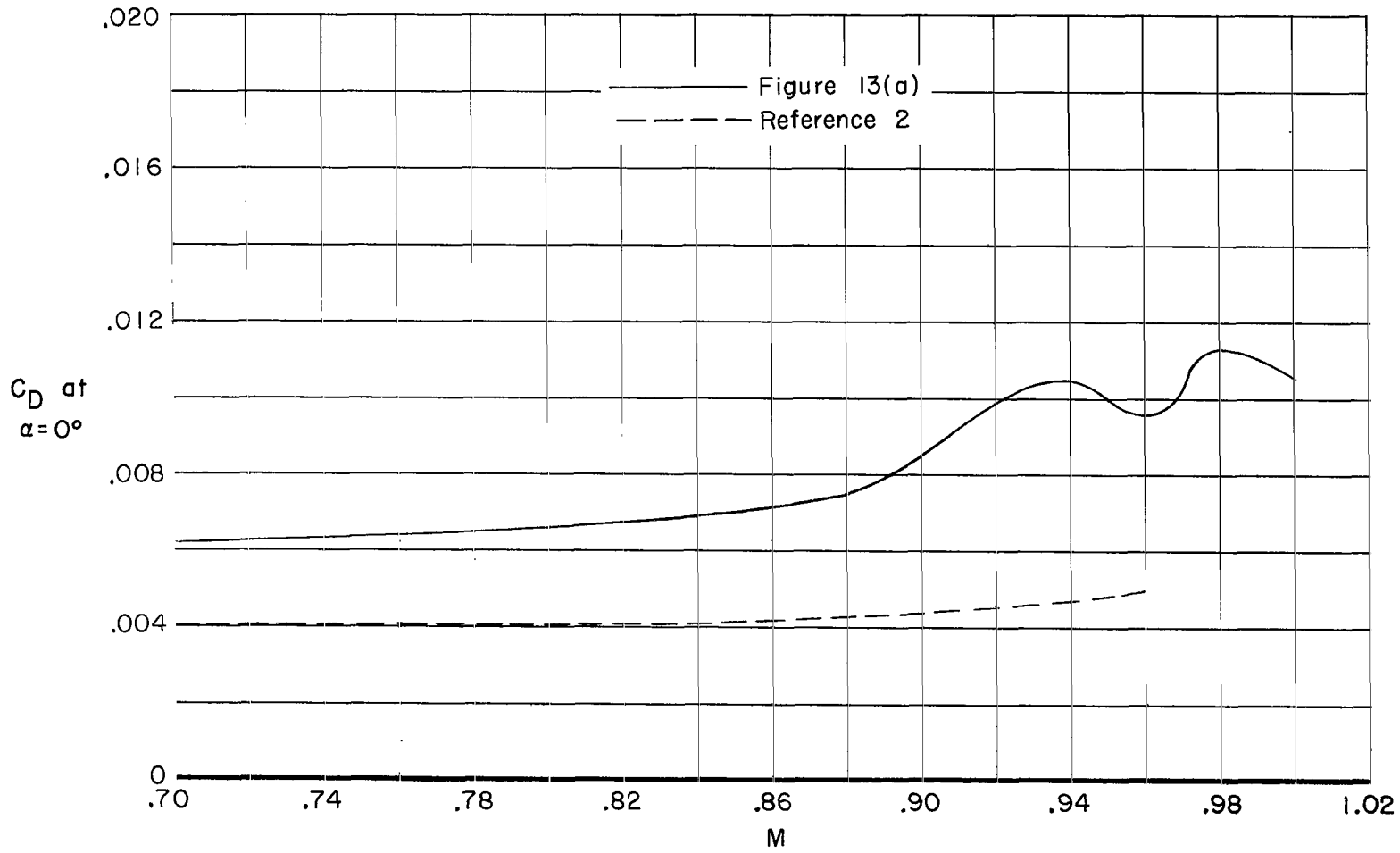

Figure 14.- Variation of drag coefficient at $\alpha = 0^0$ with Mach number for the cylindrical body of the present investigation and the cylindrical body of reference 2.

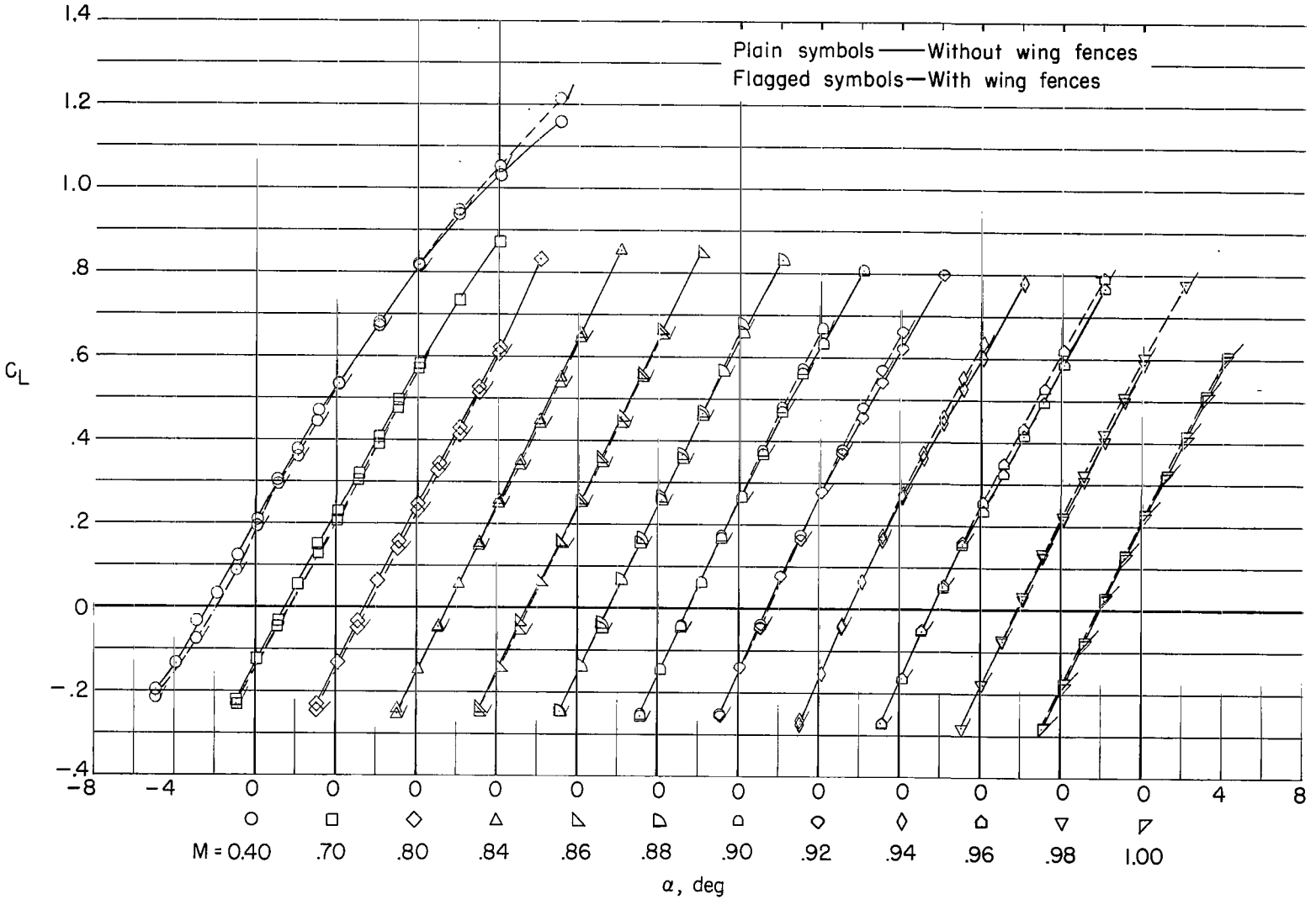

(a) Lift coefficient.

Figure 15.- Longitudinal aerodynamic characteristics of the complete model ($i_t = 2^0$) with and without wing fences.

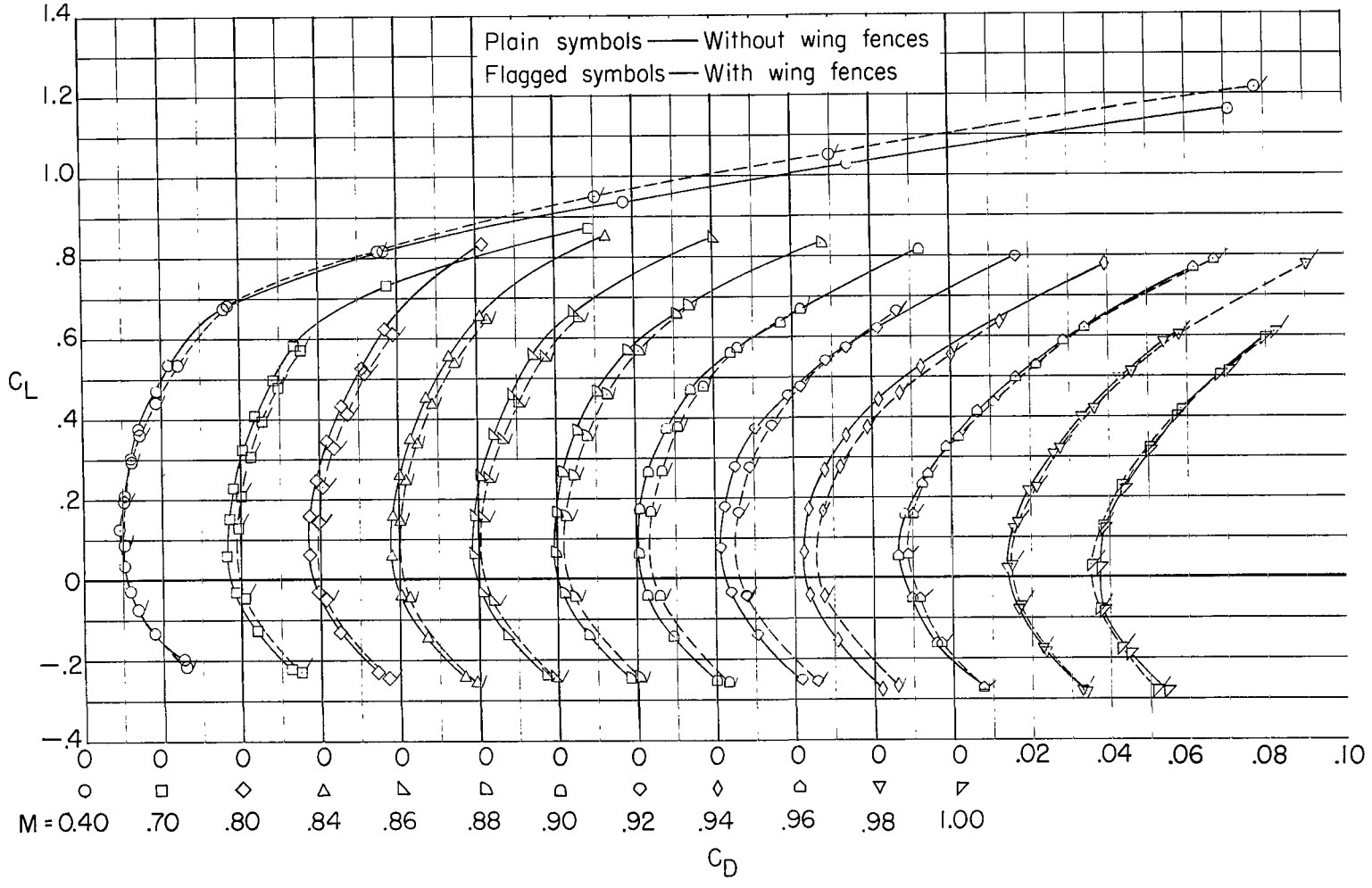

(b) Drag coefficient.

Figure 15.- Continued.

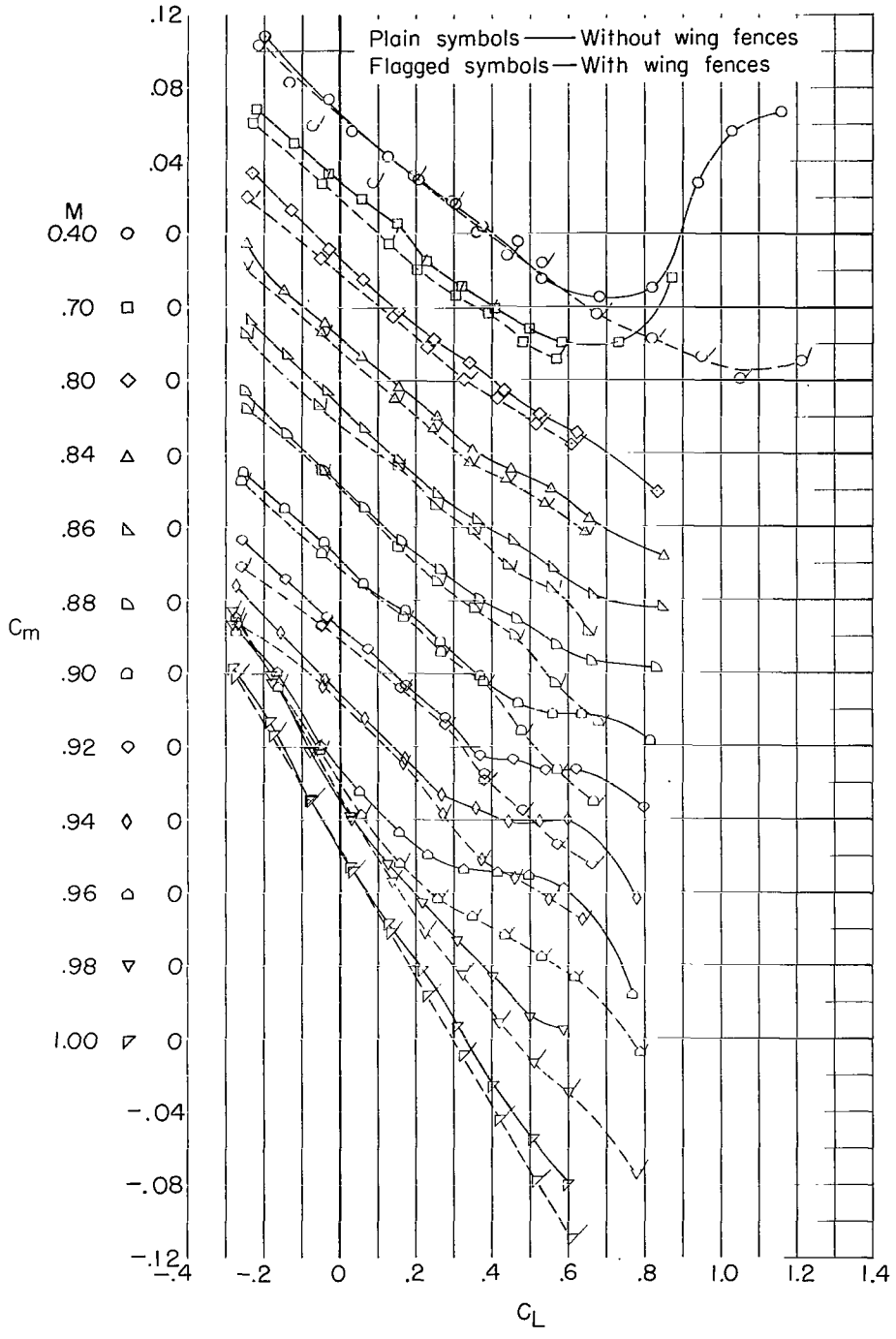

(c) Pitching-moment coefficient.

Figure 15.- Concluded.

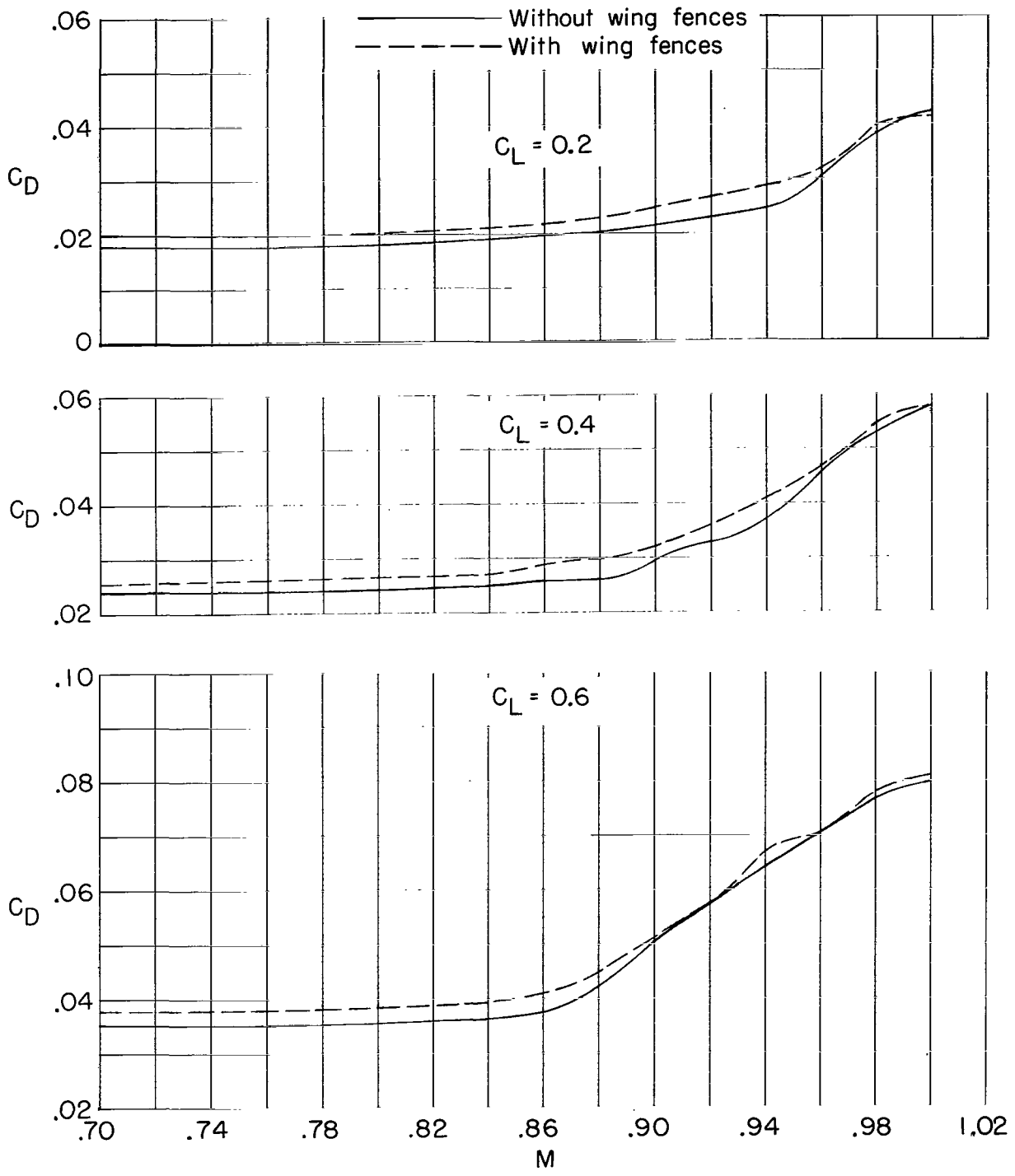

(a) Drag coefficient.

Figure 16.- Variation with Mach number of the aerodynamic characteristics of the model ($i_t = 2^0$) with and without wing fences.

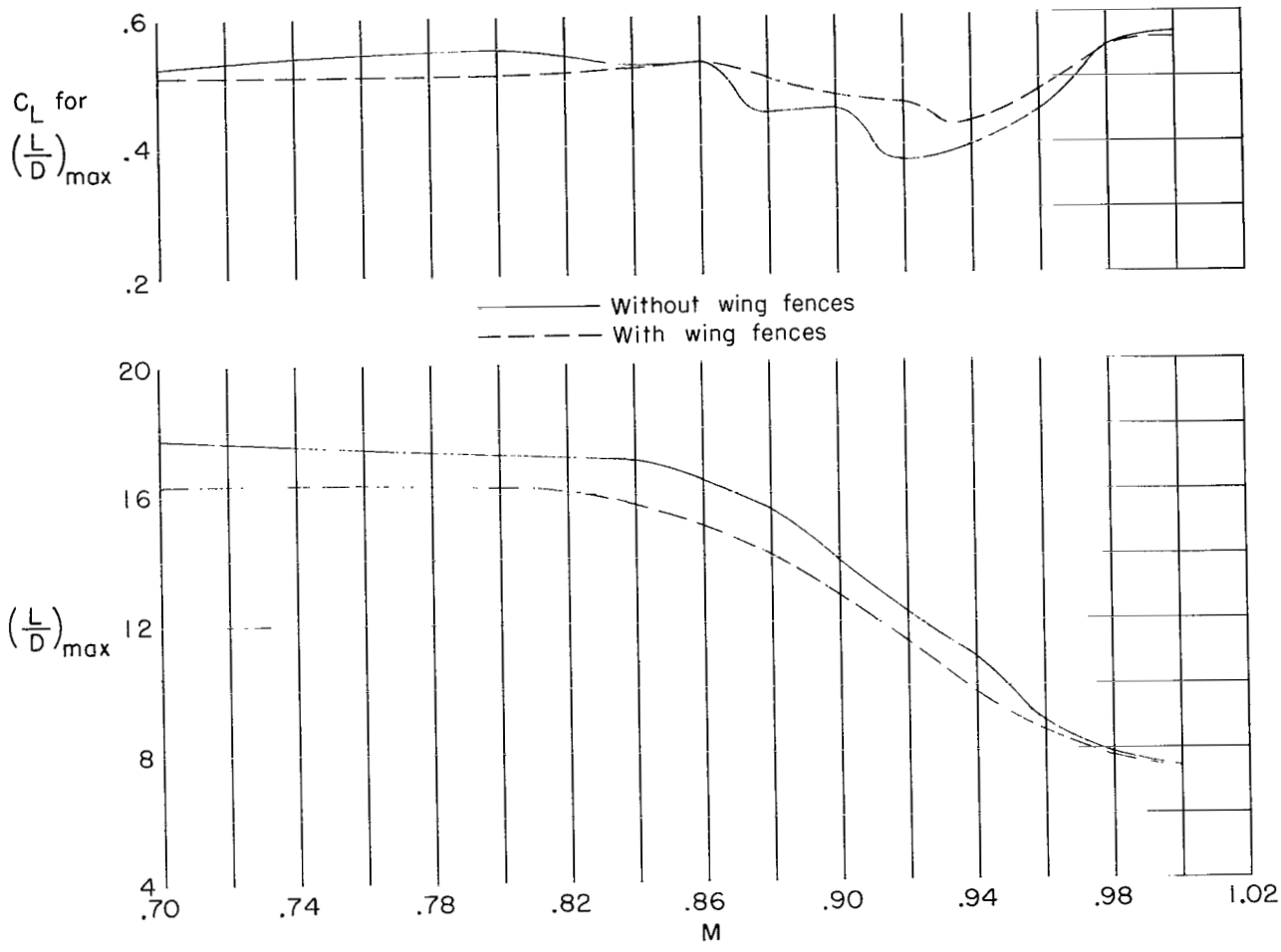

(b) Maximum lift-drag ratio and lift coefficient for maximum lift-drag ratio.

Figure 16.- Continued.

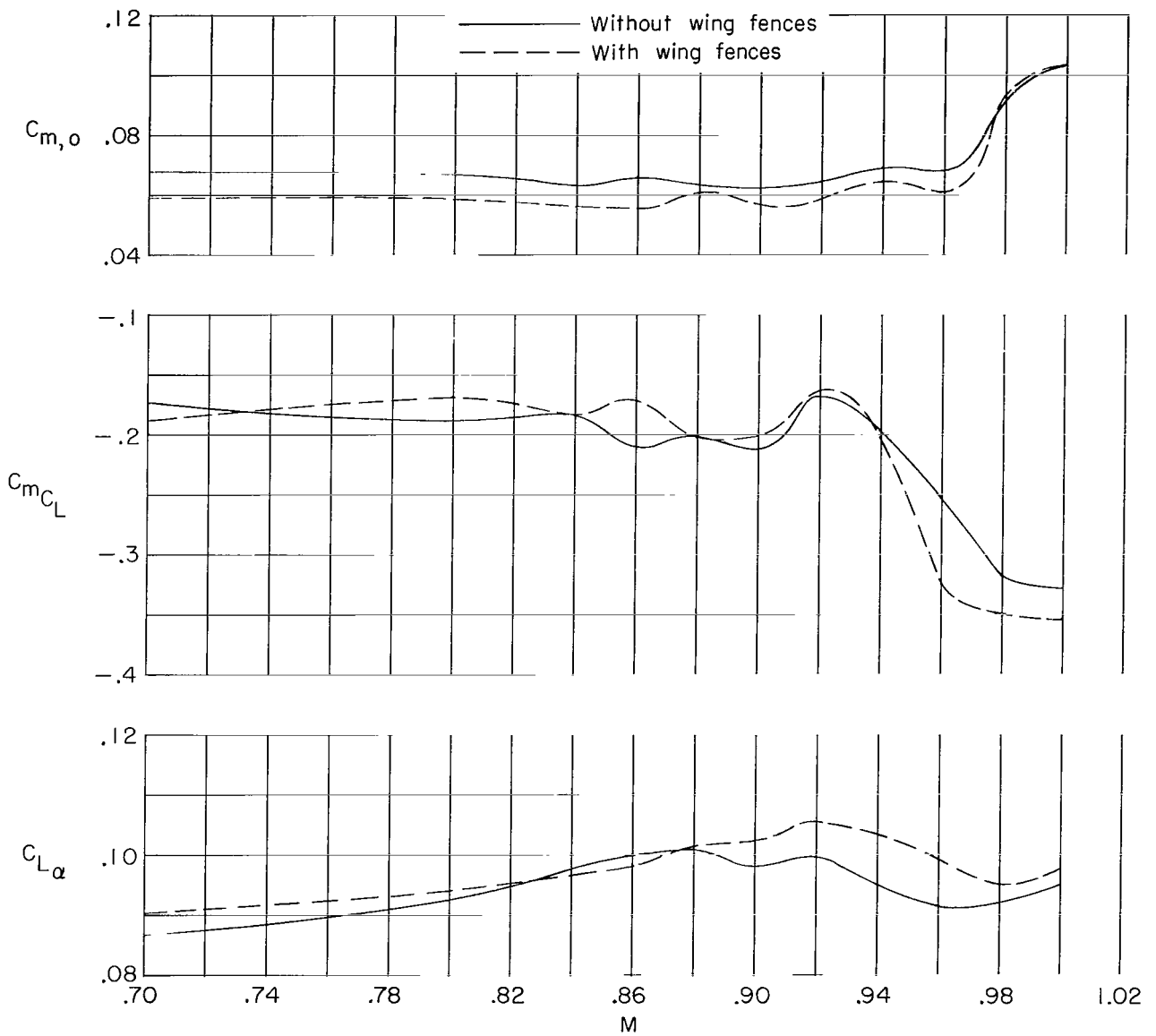

(c) Lift-curve slope, longitudinal stability parameter, and pitching-moment coefficient at zero lift.

Figure 16.- Concluded.

"The aeronautical and space activities of the United States shall be conducted so as to contribute . . . to the expansion of human knowledge of phenomena in the atmosphere and space. The Administration shall provide for the widest practicable and appropriate dissemination of information concerning its activities and the results thereof."

—NATIONAL AERONAUTICS AND SPACE ACT OF 1958

NASA SCIENTIFIC AND TECHNICAL PUBLICATIONS

TECHNICAL REPORTS: Scientific and technical information considered important, complete, and a lasting contribution to existing knowledge.

TECHNICAL NOTES: Information less broad in scope but nevertheless of importance as a contribution to existing knowledge.

TECHNICAL MEMORANDUMS: Information receiving limited distribution because of preliminary data, security classification, or other reasons.

CONTRACTOR REPORTS: Technical information generated in connection with a NASA contract or grant and released under NASA auspices.

TECHNICAL TRANSLATIONS: Information published in a foreign language considered to merit NASA distribution in English.

TECHNICAL REPRINTS: Information derived from NASA activities and initially published in the form of journal articles.

SPECIAL PUBLICATIONS: Information derived from or of value to NASA activities but not necessarily reporting the results of individual NASA-programmed scientific efforts. Publications include conference proceedings, monographs, data compilations, handbooks, sourcebooks, and special bibliographies.

Details on the availability of these publications may be obtained from:

SCIENTIFIC AND TECHNICAL INFORMATION DIVISION

NATIONAL AERONAUTICS AND SPACE ADMINISTRATION

Washington, D.C. 20546